

Controlling the mobility in nanostructured environments by stimuli-responsive polymers

Dissertation

zur Erlangung des Grades

"Doktor der Naturwissenschaften"

am Fachbereich Chemie

der Johannes Gutenberg-Universität Mainz

Jing Xie

geboren am 29.04.1988

in Guangan (China)

Mainz – 2015

Dekan:

1. Berichterstatter:

2. Berichterstatter:

Tag der mündlichen Prüfung: 11.02.2016

Die vorliegende Arbeit wurde im Zeitraum von Oktober 2012 bis Februar 2016 am Max-Planck-Institut für Polymerforschung, unter der Betreuung von ... und ... angefertigt.

Table of Contents

Abstract	9
Zusammenfassung	10
CHAPTER 1 Introduction	11
1.1 Diffusion.....	11
1.1.1. Fick's laws	12
1.1.1.1 Fick's first law	12
1.1.1.2 Fick's second Law	13
1.1.2 Einstein-Smoluchowski relation.....	15
1.1.3 Applications.....	18
1.2. Stimuli-responsive polymers	18
1.2.1 Thermo-responsive polymers	19
1.2.1.1 Poly(<i>N</i> -isopropylacrylamide)	19
1.2.1.2 The lower critical solution temperature	20
1.2.1.3 Applications	22
1.2.2 pH-responsive polymers	23
1.2.2.1 Poly(2-diethylaminoethyl methacrylate)	24
1.2.2.2 Applications	24
1.2.3 Other stimuli-responsive polymers.....	25
1.2.4 Morphology of stimuli-responsive polymers	25
1.2.4.1 Films	26
1.2.4.2 Particles.....	28
1.2.4.3 Other morphologies	30
1.3 Motivation	31
CHAPTER 2 Methods.....	33
2.1 Principle of fluorescence correlation spectroscopy (FCS)	33
2.2 FCS experimental setup.....	37
2.3 Scanning electron microscopy.....	38
2.4 pH meter	39

2.4.1 pH adjustment.....	39
2.5 Gel permeation chromatography	39
2.6. Materials.....	39
2.6.1 Fluorescent dyes	39
2.6.1.1 Alexa series.....	41
2.6.1.2 Bodipy	42
2.6.1.3 Quantum dots.....	43
2.6.2 Silica inverse opals.....	44
2.6.2.1 Silica and PS nanoparticles.....	45
2.6.2.2 Preparation.....	45
2.6.3 PS/PDEA hairy nanoparticles and PDEA single chains	48
2.6.4 Cells for FCS measurement.....	48
2.7 Atom transfer radical polymerization (ATRP).....	49
2.7.1 “Grafting from”	53
2.7.2 “Grafting to”	54
CHAPTER 3 Temperature controlled diffusion in PNIPAM modified silica inverse opals	55
3.1 Introduction and motivation	55
3.2 Atom transfer radical polymerization on silica inverse opals	58
3.2.1 Preparation of the silica inverse opals	58
3.2.2 ATRP on silica inverse opals	59
3.2.2.1 Materials	59
3.2.2.2 Initiator immobilization.....	60
3.2.2.3 Surface-initiated polymerizations.....	60
3.3 Dyes and solvents for FCS measurement.....	63
3.4 Alexa 647 and QD 525 diffusion in PNIPAM grafted silica inverse opals	63
3.5 Tuning (controlling) the penetrant diffusion.....	67
3.6 Conclusion.....	69
CHAPTER 4 pH controlled diffusion of hairy nanoparticles	71
4.1 Introduction and motivation	71

4.2 Preparation of Bodipy labeled PS/PDEA hairy nanoparticle and PDEA single chain	74
4.3 Monitoring the pH-responsive behavior at high concentration.....	76
4.4 Monitoring the pH-responsive behavior at individual particle level.....	79
4.5 Comparison of the pH-responsiveness of the hairy nanoparticles and single chains	83
4.6 Controlling the mobility of the pH-responsive particles in nanoporous environment	85
4.7 Conclusion.....	89
CHAPTER 5 Summary and conclusion	91
Acknowledgement.....	93
List of symbols	95
List of abbreviations	97
References	99
Curriculum Vitae.....	109

Abstract

Understanding and controlling the diffusion of small molecules, macromolecules and nanoparticles in solution and complex, nanostructured environments is of paramount fundamental and technological importance. Often, diffusion is the dominant mechanism for the transport of such species in e.g. solid nanoporous structures, polymer solutions and gels, or in living cells. Thus, it is relevant for many processes and applications including drug delivery, cell nutrition, porous chromatography, polymer synthesis and separation, treatment of waste water, oil recovery, etc. For all of those applications, one prerequisite is that the mobility of the species needs to be controllable. To control the mobility of the species, the size of the species itself or the size and/or density of the nanopores of surrounding environment can be changed. Stimuli-responsive polymers are ideal candidate materials to construct both systems, as they are capable of conformational changes when they are exposed to external stimuli. In addition, they can form versatile configurations such as mixed polymer brushes, micelles, vesicles, layer-by-layer films, and so on, which provides a feasible way to construct the responsive species or the responsive environment for mobility control.

For observation of species' mobility, fluorescence correlation spectroscopy (FCS) technique is a well-developed technique. The fluorescent intensity fluctuations caused by the diffusion of the species through a very small confocal detection volume are recorded and the change process can be traced. Because of its extremely small detection volume ($V < 10^{-15}$ L), high sensitivity is reached and even single molecule can be traced in the solution. Nowadays FCS has been developed as a powerful technique for studying the dynamics of fluorescent species such as small molecules, macromolecules, or nanoparticles in various environments in polymer and colloid science.

In this thesis, the species' mobility has been controlled by combining stimuli-responsive polymers. For the stimuli-responsive polymers, I choose a typical thermo-responsive polymer and a pH-responsive polymer, as they are the most classic and widely used polymers in material science and biology. FCS is used to monitor the mobility of the species in solution and also in porous media.

In the first part of this thesis, the species mobility has been controlled by changing the pore size of the surrounding medium. Poly(*N*-isopropylacrylamide) (PNIPAM) is grafted onto the well-defined, highly ordered porous network-silica inverse opal. When temperature increases above the lower critical solution temperature of PNIPAM, PNIPAM chains collapse accordingly, resulting in an increase of the mobility of the penetrant in the system, and vice versa.

In the second part of this thesis, the mobility of the nanoparticles has been controlled by changing the size of the nanoparticle itself. I prepare pH-responsive nanoparticles, which are composed of pH-insensitive polystyrene cores and pH-responsive poly (2-diethylaminoethyl methacrylate) (PDEA) hairs. When the pH increases, the PDEA hairs collapse and the size of the hairy nanoparticle will decrease, which results in faster mobility of the nanoparticles in the solution. The effect is particularly evident when the nanoparticles are dispersed in a nanostructured environment.

Zusammenfassung

Verständnis und Kontrolle der Diffusion von kleinen Molekülen, Makromolekülen und Nanopartikeln in Lösung und nanostrukturierter komplexer Umgebung sind von fundamentaler und technologischer Relevanz. Die Diffusion ist der dominierende Transportmechanismus solcher Teilchen (z. B. in festen nanoporösen Strukturen, Polymerlösungen, Gelen oder in lebenden Zellen). Die Diffusion ist daher für viele Prozesse und Anwendungen wie Wirkstofffreisetzung, Zellernährung, Chromatographie, Polymersynthesen, Aufbereitung von Abwasser oder Rückgewinnung von Öl relevant. Durch die Kontrolle der Größe der Teilchen, der Dichte oder Größe der nanoporösen Umgebung ist es möglich, die Bewegung der zu untersuchenden Teilchen zu kontrollieren. Ideale Materialien zur Herstellung dieser Systeme sind stimuliresponsive Polymere. Sie reagieren auf spezifische Anregungen und können abhängig von externen Reizen ihre Konformation ändern. Außerdem können sie verschiedenste Konfigurationen annehmen, wie z. B. Bürstenpolymere, Mizellen, Vesikel, geschichtete Filme, usw. Durch externe Reize ist es möglich, die Mobilität zu kontrollieren.

Zur Beobachtung der Teilchenbewegung eignet sich die Fluoreszenzkorrelationsspektroskopie (FCS – engl. fluorescence correlation spectroscopy). Dabei diffundieren die fluoreszierenden Teilchen durch ein sehr kleines konfokales Detektionsvolumen. Die Intensitätsfluktuation der Fluoreszenz wird aufgenommen und ausgewertet. Durch das sehr geringe Detektionsvolumen ($V < 10^{-15}$ L) und die hohe Sensitivität der Methode, können sogar einzelne Moleküle in der Lösung detektiert werden. Heutzutage ist FCS eine häufig genutzte und sehr gute Methode zur Untersuchung der Dynamik von fluoreszierenden Teilchen wie kleinen Molekülen, Makromolekülen oder Nanopartikel in verschiedensten Bereichen der Polymer- und Kolloidwissenschaft.

In der vorliegenden Arbeit wird die Mobilität der Teilchen durch die Kombination von stimuliresponsiven Polymeren kontrolliert. Hierfür werden auf Temperatur reagierende Polymere mit pH-abhängigen Polymeren kombiniert, da diese zu den klassischen und häufig verwendeten Polymermaterialien im Bereich der Biologie zählen. Zur Beobachtung der Mobilität dieser Teilchen in Lösungen als auch in porösem Material wird FCS verwendet.

Im ersten Teil der Doktorarbeit wird die Teilchenbewegung durch die Veränderung der Porengröße des umgebenden Mediums kontrolliert. Poly(*N*-Isopropylacrylamid) (PNIPAM) wird dafür auf einen inversen Opal mit hoch geordnetem porösen Silicanezwerk aufgepfropft. Aufgrund von Temperaturerhöhung über die untere kritische Lösungstemperatur (LCST – engl. lower critical solution temperature) von PNIPAM, kollabiert die Polymerkette und verursacht eine Erhöhung der Teilchenbewegung im System, und umgekehrt.

Im zweiten Teil der Doktorarbeit wird die Mobilität von Nanopartikel durch Veränderung der Partikel selbst kontrolliert. Nanopartikel aus pH-stabilem Polystyrol-Kern und pH-abhängigen Polymerbürsten aus Poly(2-Diethylaminoethylmethacrylat) (PDEA) wurden dafür hergestellt. Wird der pH-Wert erhöht, kollabieren die PDEA-Bürsten und die Größe des Partikels verringert sich, was zu schnellerer Teilchenbewegung in der Lösung führt. Dieser Effekt zeigt sich besonders deutlich, wenn die Nanopartikel in nanostrukturierter Umgebung verteilt sind.

CHAPTER 1

Introduction

1.1 Diffusion

Diffusion is the spontaneous transport of mass in gases, liquids and solids from a high concentration to low concentration, until equilibrium is finally reached in the whole system. Diffusion is an irreversible process which leads to an increase in entropy and can only be reversed by other work. It happens in solid, liquid and air phases, and exists everywhere in our daily life. For example, we can smell the fragrance of the flowers even though we don't go close to the garden; a droplet of ink can dye a whole solution even though we do not stir the solution. Diffusion has been used long time before its scientific investigation, such as the diffusion of colors of earthenware and Chinese ceramics. It has caught scientific attention in the 19th century, since the Scottish botanist Robert Brown observed that pollen moves through water. "Brownian motion" was named to commemorate his contribution to first describe the diffusion. In his observation, no concentration gradient exists in water but the pollen can also move, which is different from the irreversible diffusion. In 1905, Albert Einstein published a paper and explained in precise details how the motion that Brown had observed was a result of the pollen being moved by individual water molecules.[1] This explanation is about the pollen moves inside the water got different force from all the directions by the water molecule, which makes it randomly move in the water. During the same period, German physicist Adolf Fick introduced Fick's laws of diffusion, which govern e.g. the diffusion of a gas across a fluid membrane.[2] Fick's second law is also called the diffusion equation. Depending on the type of diffusing species and the fluid medium as well as the length scale, there are different types of diffusion, i.e. molecular diffusion (gas and liquid), Knudsen diffusion (gas), surface diffusion (lateral diffusion) and

configurationally diffusion (pore diameter within molecular dimensions 0.3-1 nm). In this thesis, I would only consider the molecular diffusion, especially the molecular diffusion in fluids. In order to describe the diffusion clearly, I would first introduce the collective diffusion manifested by Fick's laws; and then self-diffusion manifested by Einstein-Smoluchowski relation.

1.1.1. Fick's laws

Inspired by diffusion of gas reported by Thomas Graham, Fick looked into the salt-water system.[3] The concept of the diffusion was introduced by Fick, the one-dimensional diffusion and three-dimensional diffusion were both included, and the particle diffusion equation was originally derived. It rose up the fundamental theory of diffusion and encouraged the subsequent research.

1.1.1.1 Fick's first law

Fick's first law assumes the steady state of the diffusive flux. This means that the flux is directed from regions of high concentration to regions of low concentration, along with an average concentration gradient. In one dimension, this can be expressed by

$$J = -D \frac{\partial C}{\partial x} \quad (1.1)$$

Here J is the flux; it means the amount of substance that will flow through an infinitely small area during an infinitely small time interval. Its unit is quantity per unit area per unit time, like mol/m²s. D is the diffusion coefficient, its unit is the surface per time, m²/s; C is the concentration which changes along the length x. The negative sign indicates the opposite directions of diffusion flux and concentration gradient.

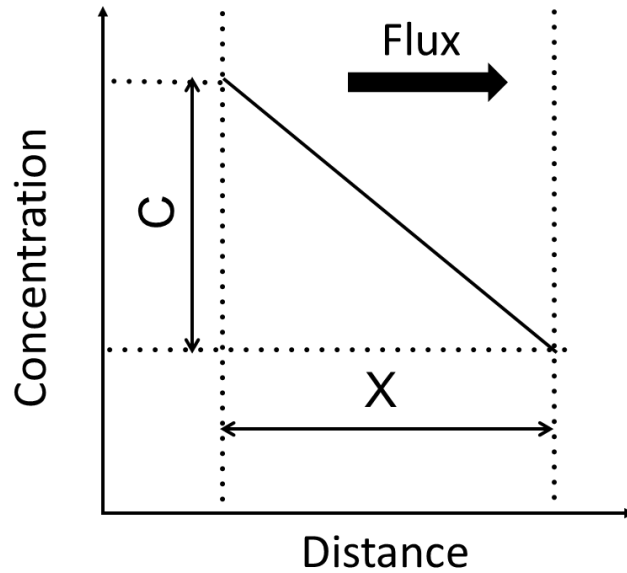


Figure 1.1. Illustration of Fick's first law

In two or more dimensions I use the gradient operator ∇ ,

$$J = -D\nabla C \quad (1.2)$$

1.1.1.2 Fick's second Law

Fick's second law predicts how diffusion changes the concentration with time, for example, the diffusion occurs in a chemical composition gradient. In the following, we first introduce the Fick's second law in one dimension.

I choose an arbitrary point P located at (x, y, z) and an infinitely small test volume with the dimension $V = \Delta x * \Delta y * \Delta z$. As the diffusion flux J passes through point P, J can be separated into its three special components, J_x , J_y and J_z . For simplification, I only look at the x direction.

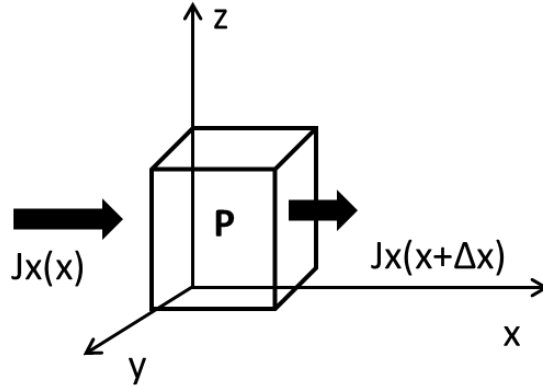


Figure 1.2. Infinitesimal test volume. The in- and outgoing x-components of the diffusion flux are indicated by arrows.

If the sum of the fluxes leaving and entering the test volume does not balance, a net accumulation (or loss) must occur. This material balance can be expressed as

$$\text{Inflow/time} - \text{outflow/time} = \text{accumulation (or loss) rate}$$

The equation can be rewritten using the flux

$$[J_x(P) - J_x(P + \Delta x)] = \text{accumulation (or loss)}$$

Using the flux components up to their linear terms, the expressions in square brackets can be replaced by $\Delta x \frac{\partial J_x}{\partial x}$. This yields:

$$- \left[\frac{\partial J_x}{\partial x} \right] \Delta x = \frac{\partial c}{\partial t} \Delta x \quad (1.3)$$

Where the accumulation (or loss) in the test volume is expressed in terms of the partial time derivative of the concentration. Removing common divisor Δx we can get:

$$- \left[\frac{\partial J_x}{\partial x} \right] = \frac{\partial c}{\partial t} \quad (1.4)$$

If we consider the three-dimension, for an infinitesimal size of the test volume, Equation 1.4 can be written in compact form by introducing the vector operation divergence ∇ . The gradient vector Nabla acts on the vector of the diffusion flux:

$$-\nabla J = \frac{\partial C}{\partial t} \quad (1.5)$$

By plugging Equation 1.5 in Fick's first law, we can infer that:

$$\begin{aligned} \frac{\partial C}{\partial t} &= \nabla \left(D \frac{\partial C}{\partial x} \right) \\ &= D \frac{\partial^2 C}{\partial x^2} \end{aligned} \quad (1.6)$$

Where C is the concentration with the dimensions of [(amount of substance) length⁻³], for example, mol/m³, $C=C(x, t)$ is a function that depends on location x and time t , D is the diffusion coefficient in dimensions of [length² time⁻¹], for example m²/s.

In two or more dimensions we must use the Laplace operator $\Delta = \nabla^2$, which generalizes the second derivative to obtain the equation

$$\frac{\partial C}{\partial t} = D \Delta C \quad (1.7)$$

1.1.2 Einstein-Smoluchowski relation

As described before, Robert Brown observed that pollen can move through water even though there are not pollen concentration gradients in solution. In 1905, Einstein and Smoluchowski[4] independently published works on Brownian motion. Contrary to collective diffusion induced by density gradients, which involves the transport of particles, self-diffusion is related to the dynamics of a single particle in a system with homogeneous density. To simplify the following derivation, I limit it to the one-dimensional case.

Suppose one fixed, external potential U exerts force on a particle

$$F = -\frac{\partial U}{\partial x} \quad (1.8)$$

The particle would react, by moving with a velocity

$$v = \mu F \quad (1.9)$$

μ is the mobility of the particle's terminal drift velocity to an applied force.

Assuming that there is a large number of such particles with a local concentration $\rho(x)$ as a function of position, the concentration will equilibrate: the particles will stay in the areas with lowest U , but will still be spread out to some extent because of random diffusion. At this point, there is no net flow of particles: the tendency of particles to get pulled towards lower U , called the "drift current" should be equal to opposite the tendency of particles to spread out due to diffusion, called the "diffusion current".

The flow of particles due to the drift current alone is

$$J_{drift}(x) = \mu F(x)\rho(x) = -\rho(x)\mu \frac{\partial U}{\partial x} \quad (1.10)$$

The flow of particles due to the diffusion current alone is, by Fick's laws

$$J_{diffusion}(x) = -D \frac{d\rho(x)}{dx} \quad (1.11)$$

As there is no net flow of particles, we can get:

$$0 = J_{drift} + J_{diffusion} = -\rho(x)\mu \frac{\partial U}{\partial x} - D \frac{d\rho(x)}{dx} \quad (1.12)$$

From thermodynamics- Boltzmann statistics, we know:

$$\rho(x) = Ae^{-U/(k_B T)} \quad (1.13)$$

k_B is Boltzmann's constant, T is the absolute temperature. As A is some constant related to the total number of particles, so:

$$\frac{d\rho(x)}{dx} = -\frac{1}{k_B T} \frac{\partial U}{\partial x} \rho(x) \quad (1.14)$$

Finally, plugging Equation 1.14 in Equation 1.12:

$$0 = J_{drift} + J_{diffusion} = -\rho(x)\mu \frac{\partial U}{\partial x} + \frac{D}{k_B T} \frac{\partial U}{\partial x} \rho(x) = -\rho(x) \frac{\partial U}{\partial x} \left(\mu - \frac{D}{k_B T}\right) \quad (1.15)$$

Since this equation must be reached, we can get the standard Einstein-Smoluchowski relation:

$$\mu = \frac{D}{k_B T} \quad (1.16)$$

When the diffusing species are spherical particles which moves through a liquid, we get

$$D = \frac{k_B T}{6\pi\eta r} \quad (1.17)$$

η is the dynamic viscosity, r is the radius of the spherical particle.

For self-diffusion the single particle under consideration is called tracer particle, while the remaining particles are referred to as host particles. The single particle suspended in a liquid, surrounding by lots of water molecules. According to thermodynamics water molecules are randomly moving in solution and collide with the single particle, because of different force from each direction, the single particle moves randomly in solution.

To quantify the motion of a single Brownian particle, its mean squared displacement is defined as

$$\langle \Delta r^2(\tau) \rangle = 6D_s(\tau)\tau \quad (1.18)$$

Equation 1.18 shows that for the particle with diffusion coefficient D_s at time interval τ , the displacement the particle can reach. Self-diffusion coefficient characterizes the stochastic motion of tracer particles.

1.1.3 Applications

As described above, diffusion is relevant for many applications including drug delivery, polymer synthesis, cell nutrition, etc. Studying the mechanism of diffusion and correlating it with other controlled environment has been a major research topic in recent years. Nowadays, many models and equations are built and people are exploring new ways to tune the diffusion behavior. Highly developed model systems satisfy more application requirements. Can we speed up the chromosomes mobility when it's transported? Or can we slow down the drug release when medicine is taken? People wish they can realize tuning the diffusion behavior according to the specific requirement, as it shows quite a lot of the practical application in biology and industry. Complex, organic- inorganic hybrids are introduced to the diffusion system. Among newly developed materials, stimuli-responsive polymers are ideal candidate materials to form such systems. Stimuli-responsive polymers can change their configuration when a stimulus is acting on them and can also be organized in versatile morphologies. Thus these materials can be used to decorate either the diffusants themselves or the surrounding environment. In the next subchapter, I would mainly introduce the basic information of versatile stimuli-responsive polymers.

1.2. Stimuli-responsive polymers

Stimuli-responsive polymers have attracted wide interest in the past 20 years, as they play an important role in building smart and controllable nano-objects owing to their natural advantages.[5] Firstly, the size of the polymer chains ranges in the nanometer scale. Secondly, polymers show diversified configurations like linear, star-like, dendritic, comb-shaped and cross-linked structures. Moreover, they can also self-assemble into different structures.[6] Thirdly, because of their vast possibilities of functionalities, polymers can respond to different external or internal stimuli. In detail, stimuli can be divided into three main kinds - chemical, physical and biological stimuli.

In the following chapter, thermo and pH-responsiveness, the most typical physical and chemical responsiveness in nature are described in details.

1.2.1 Thermo-responsive polymers

Among all the stimuli, temperature remains the most extensively exploited stimuli in the field of responsive polymers, as it is an easy stimulus to apply.[7] Thermo-responsive behavior can be induced in a variety of settings, including *in vivo*, and potential benefits have been envisioned for a range of biologically relevant applications, including controlled drug delivery, bioseparation, filtration, smart surfaces, and regulating enzyme activity.

1.2.1.1 Poly(*N*-isopropylacrylamide)

Poly(*N*-isopropylacrylamide) (PNIPAM) has drawn significant attention as the most commonly used thermo-responsive polymer (Figure 1.3a). In 1967 it has been reported for the first time by Scarpa et al. as the thermal phase transition polymer.[8] At room temperature and normal pressure, due to extensive hydrogen bonding interactions with the surrounding water molecules, the responsive polymer is soluble. Meanwhile intra- and intermolecular hydrogen bonding between polymer molecules were restricted because of the strong hydrogen bonding interactions with the surrounding water molecules. Upon heating, hydrogen bonding with water is disrupted, and intra- and intermolecular hydrogen bonding/hydrophobic interactions dominate, which results in a transition in solubility, as shown in Figure 1.3b.[9] This can be explained from thermodynamic view.[10] Considering the free energy of the system by using the Gibbs equation:

$$\Delta G = \Delta H - T\Delta S \quad (1.20)$$

G is Gibbs free energy, H is enthalpy and S is entropy. When increasing the temperature, the phase separation is more favorable due to the entropy contribution of

the system. Specifically, when the polymer is not in solution the water is less ordered and has higher entropy. Up to now, PNIPAM based response materials have been used in many applications including permeability switching membrane[11], adhesion to biomolecules adjusting hydrogels[12] and self-healing hydrogels[13].

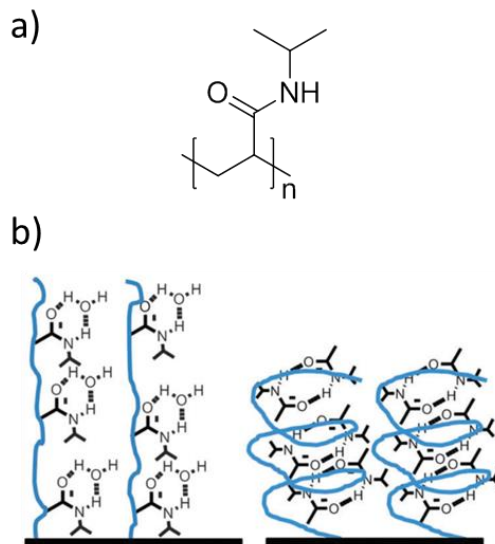


Figure 1.3. (a) Chemical structure of PNIPAM. (b) Schematic illustration of hydrophilic and hydrophobic states of PNIPAM because of different hydrogen bonding effect.

Reproduced from Ref. 9 with permission from The Royal Society of Chemistry.

1.2.1.2 The lower critical solution temperature

There are two main types of thermo-responsive polymers: one kind has the lower critical solution temperature (LCST) and the other kind has upper critical solution temperature (UCST). LCST is the critical temperature below which the components of a mixture are miscible for all compositions. When the polymer stays at the temperature below LCST, the polymer is miscible with the solvent; when the polymer stays at the temperature above LCST, it becomes partially immiscible with the solvent, as shown in Figure 1.4[14]. There are also some polymers with high UCST, which are dissolving better at the temperature above UCST. Here I would focus on the polymers which have

LCST. LCST is not fixed for one kind of polymers; moreover, the LCST can be readily tuned.[7] Firstly incorporating hydrophilic or hydrophobic character can adjust LCST. By increasing the hydrophilic nature of the polymers, the overall hydrogen bonding ability of the macromolecules is increased, which leads to higher transition temperatures. Vice versa, incorporating hydrophobic groups lowers the LCST. For example, the LCST of PNIPAM is around 31 °C[15], which is conveniently between room and body temperatures. By the incorporation of comonomers or hydrophilic groups, the LCST can be adjusted to increase body temperature, which makes PNIPAM (co)polymers a prominent candidate in biomedical applications.[16] Secondly, concentration can also have an impact on LCST.[17] For example, PNIPAM exhibit decreasing thermal transitions with increasing concentrations, which is caused by undergoing intra- and intermolecular hydrogen bonding. Thirdly, salt in solution would also have an effect on LCST, depending on its type and the concentration. Normally the anions have a greater effect on solubility than cations, even though the mechanism is not clear yet. Last but not least, the versatile outer condition would also change the LCST a lot, like co-solvents, surfactants.[18] Moreover, the same polymer chain may behave different when it is as free chain or grafted onto the flat surface or the curved surface. This also becomes a hot topic for the investigation of polymers.

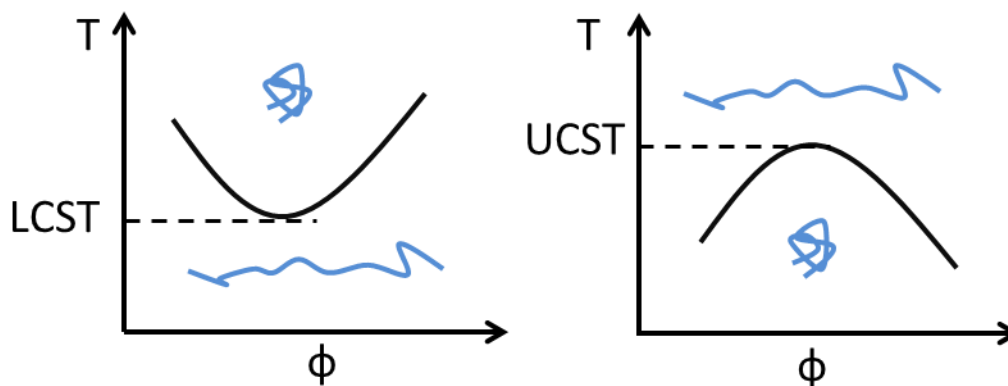
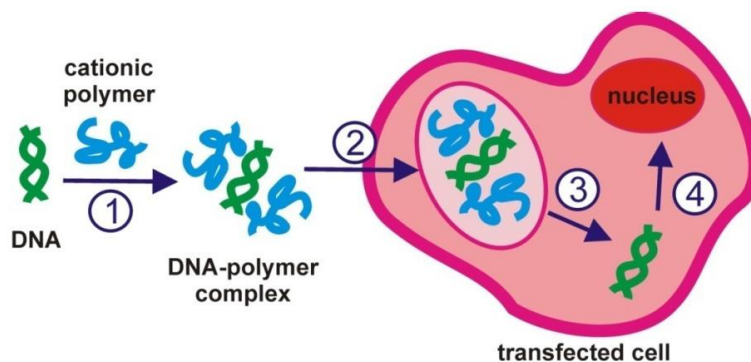


Figure 1.4. Scheme of the phase transition associated with LCST (lower critical solution temperature) and UCST (upper critical solution temperature) behavior. The black lines

represent the phase separation boundary or cloud point at which the solutions become hazy. The blue curves are the polymers chains in the collapse or swollen state.

1.2.1.3 Applications

Up until now, temperature remains the most extensively exploited stimuli in the field of responsive polymers. Thermo-responsive behavior can be induced in a variety of settings, including switching the film permeability[19], wetting properties[20], and a range of biologically relevant applications, including controlled drug delivery, bioseparations, tissue, engineering, filtration, smart surfaces, adhesion to biomolecules[21], and so on. Here I use Scheme 1.1 to show how thermo-responsive polymer is used for gene delivery.



Scheme 1.1. Four main steps of gene delivery: (1) DNA complexion (2) complex traversing the cell membrane to the cytoplasm (3) DNA release into the cytoplasm and (4) DNA transfer into nucleus. This picture is reprinted from Ref 10 (Polymers 2011, 3, 1215-1242).

DNA is negatively charged, and cell membrane is also negatively charged, what makes it difficult to realize if it is needed to pass through the cell membrane. Therefore, gene delivery vehicles are developed. Polymer based carriers are popular as they show biocompatibility and easy tailed property. For thermo-responsive polymers they also have another important function-enhancement of transfection efficiency. This can be

realized by changing temperature during the complexation or during the incubation or transfection period. Zhou group use PNIPAM based star polymers as a gene transfection.[22] They complex DNA and polymers at the temperature below the LCST then deposit the complex on a surface above the LCST. This can result higher transfection to cells cultured on the surface.

1.2.2 pH-responsive polymers

pH-responsive polymers are a kind of polymers which show configuration transition as the surrounding pH condition changes.[23] In general, pH-responsive polymers contain either acid or base segments. When these polymers are fully neutralized, they can be transformed to polyelectrolytes or polyampholytes. The protonation and deprotonation of the functional group can also cause the pH induced configuration. As different cells in vivo require different acid-basic balanced solutions [18], as shown in Table 1.1, it's becoming extremely important to develop pH-responsive polymers with biocompatibility and antibacterial activity for the biological application.

Table 1.1. Summary the requirements of specific pH condition of the biological system. This table is reprinted from Ref 18(Advanced Drug Delivery Reviews, 2006, 58, 1655–1670).

Tissue/cellular compartment	pH
Blood	7.35–7.45
Stomach	1.0–3.0
Duodenum	4.8–8.2
Colon	7.0–7.5
Early endosome	6.0–6.5
Late endosome	5.0–6.0
Lysosome	4.5–5.0
Golgi	6.4
Tumour, extracellular	7.2–6.5

1.2.2.1 Poly(2-diethylaminoethyl methacrylate)

Poly(2-diethylaminoethyl methacrylate) (PDEA) is a pH-responsive polymer with biocompatibility and low toxicity.[23] PDEA shows controlled molecular weights, well-defined chain ends, different macromolecular architectures and functionalities.[24] The pK_a of PDEA is around 7.3, depending on molecular weight. Different architectures like block, star, and graft, can be realized by controlled radical polymerization such as atom transfer radical polymerization (ATRP) and reversible addition fragmentation transfer (RAFT). In aqueous solutions of both star-shaped and linear PDEA, the cloud point can be readily tuned by changing the pH of the solution and the molecular weight and concentration of the polymer. Figure 1.5 shows the molecular structure of PDEA. Due to its properties, it is used as a promising material in systems for the design and precise synthesis of advanced synthetic biomaterials in gene delivery, pH-responsive controlled release, etc.

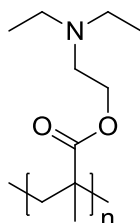


Figure 1.5. The structure of PDEA.

1.2.2.2 Applications

pH-responsive polymeric systems have been extensively studied from both the theoretical and applied perspectives.[23] Well-defined block copolymers resulting in the formation of nanostructured particles or polymeric brushes can be produced with controlled polymerization techniques. In aqueous homopolymers systems, external pH could induce phase separation; in microgels, external pH could induce swelling/deswelling of particles; for block copolymers, pH difference would result in the

pH-responsive polymers self-assemble into aggregates of different shapes. Because of the easy configuration transition and biocompatibility of pH-responsive polymers, they show wide application in biological fields, such as drug delivery systems, enzyme immobilization, separation, chemo-mechanical systems, chemical valves, sensors, controlled releases and so on. [18, 23, 25]

1.2.3 Other stimuli-responsive polymers

Besides the thermo- and pH-responsive polymers, there are also polymers that can respond to other stimuli, like voltage, light-irradiation, or mechanical stress. In general, physical stimuli include light, pressure, etc. Among the chemical stimuli, pH value, the ionic strength, as well as the addition of chemical agents, are the most common examples. Moreover, responses to antigens, enzymes, ligands or other biochemical agents are biochemical stimuli-responsive polymers. Nowadays, the stimuli-responsive polymers are explored for their various applications including drug release, smart and self-healing coatings, tunable catalysis, biointerfaces, bioseparation and responsive filters. [5]

1.2.4 Morphology of stimuli-responsive polymers

As mentioned above, stimuli-responsive polymers can perform conformation changes on receiving an external signal change, like temperature, chemical composition, irradiation with light, etc. In order to study the architectures and fundamental approaches of stimuli-responsive polymers, generally the systems can be divided to two-dimensional and three-dimensional.[5] Films are the most typical and commonly used morphology in two-dimensional systems, including homopolymer brushes, block copolymers brushes, mixed polymer brushes, hybrid film brushes, and so on. In three-dimensional systems, particulates and their assemblies are the main part. In the following subchapter, I will introduce stimuli-responsive polymer in each system and how the transition changes exposed to the external stimuli.

1.2.4.1 Films

Films are the most commonly used morphology for the stimuli-responsive polymers. Polymer brushes, layer by layer films, hydrogel films are the main morphologies.[9] For polymer brush, one chain-end is fixed onto a solid substrate and the other side is relatively flexible and can respond to the external stimuli. Up until now, people use versatile methods to probe films such as contact angle, atomic force microscopy, ellipsometry, quartz-crystal micro-balance, infrared and neutron reflectivity. Original theories suggested that the density of the polymer chains was constant[26, 27] but later a more accurate representation with a higher density of monomer units at the substrate compared to the surface is introduced, as shown in Figure 1.6b. [28] This distinction of polymer brushes is crucial in their applications, because for the bulk transition or the surface they would behave differently and bring different results.

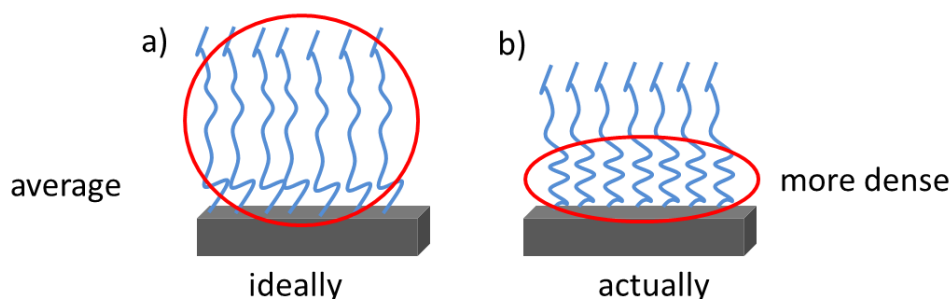


Figure 1.6. Generalized depictions of density in polymer brushes which are grafted onto the solid substrate. (A) Average chain density on the substrate; (B) denser chains close to the substrate.

Moreover, the density of the polymer on the substrate would also have an impact on the transition of the polymer, as shown in Figure 1.7[14]. A distinct transition exists between very lightly grafted polymers in the ‘mushroom’ regime compared to the densely packed ‘brush’ regime. The brush regime appears when the distance between grafting sites of the polymers is greater than twice the radius of gyration (R_g) of the individual polymers. In the mushroom regime, as the chain intensity is relatively low,

the interaction between solvent and substrate can't be ignored. Therefore, a direct consequence of this is that the hydrophilicity/hydrophobicity of the polymer corona is therefore influenced by the nature of the underlying substrate.

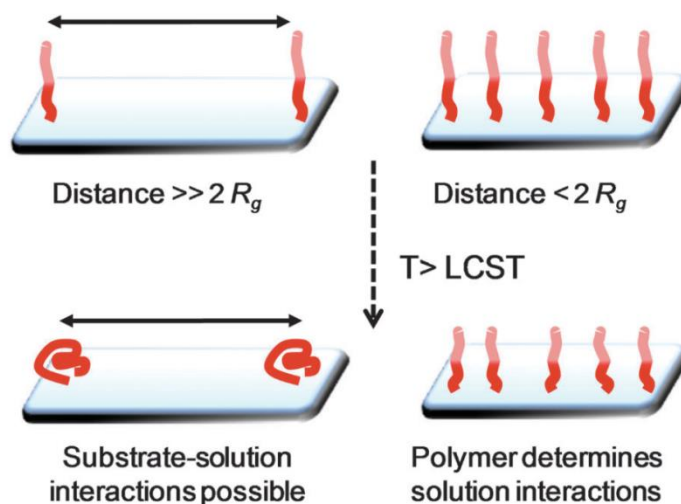


Figure 1.7. Effect of polymer brush morphology on conformation transitions above their LCST. R_g is the radius of gyration of an individual polymer chain. This picture is reprinted with permission from Ref 14.

Besides polymer brush films, network film and porous gel films are also well studied. Nanostructured thin network films are materials in which surface confinement brings a range of opportunities for engineering stimuli-responsive properties. An important attribute of gel thin films is their fast kinetics of swelling and shrinking compared with bulk gels, ranging from microseconds to seconds. The swelling-response of these films is highly anisotropic, because the attachment of the network to a surface prohibits in-plane swelling. Another important attribute of films are porous thin gel films. Switching between open and closed pores in thin gel films on shrinking and swelling, respectively, provides a unique opportunity for the regulation of transport through the film in a very broad diffusivity ranging from the level in solution down to a level in solids.

Moreover, polymer film can not only be grafted onto the flat solid surface but also grafted onto the well-defined and functional solid structure by different living radical polymerization. This guarantees the polymer with bigger flexibility. It's interesting to see how the polymer behave when the environment changes, and whether it would be different with different morphology such as free chain, onto nanoparticle or on the network.

In summary, films have obvious advantages compared to bulk morphology. First, fast responsiveness of tuning and switching adhesion between stimuli-responsive materials, proteins and cells has been explored for the control of cell and protein adhesion, which can be used for tissue engineering and bioseparation. Second, the possibility of dynamic control of the permeation of chemicals through nanoporous membranes interaction of biomolecules and ions with responsive surfaces offers a unique opportunity for bioseparation. For example, surface-grafted stimuli-responsive polymers provide an exciting means for controlling drug permeation through nano- and microporous membranes.

1.2.4.2 Particles

Particles are a widely use morphology for stimuli-responsive polymers. In general, there are two kinds. One kind is hybrid inorganic-polymer particles, which are composed of an inorganic or metal particle core and a polymer shell showing intriguing properties; the other kind is composed by various polymer types which can form versatile assemblies. For the polymers assembly, as one block shows responsive property exposing the stimuli, the swelling or contraction happens and may also induce the reversible or irreversible structural transformation among vesicles, micelles, nanogels, and so on.[6] Figure 1.8 shows the possible transformations of poly(ethylene-*alt*-propylene)-*b*-poly(ethylene oxide)-*b*-poly(*N*-isopropylacrylamide) (PEP-PEO-PNIPAM) composing triblock copolymers.[29]

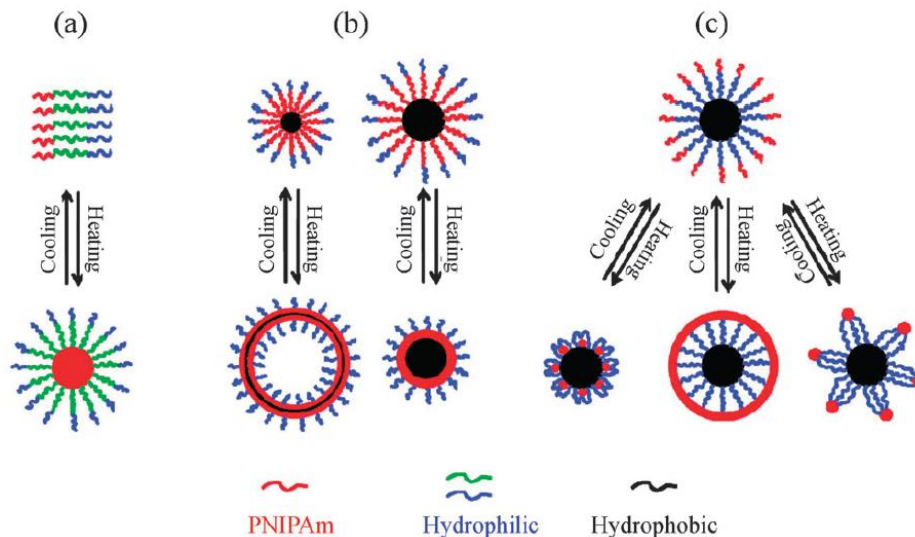


Figure 1.8. Effect of block sequence in a triblock copolymer assembly structural transformations. Reprinted with permission from Ref 29. Copyright (2011) American Chemical Society.

When polymer chains are densely tethered to the surface of particles, one end of the chain is covalently bonded, and the other side of the chain tries to stretch away from the grafting sites and extend its conformation due to the excluded volume interaction, hairy nanoparticle are generated. In particular, immobilization of polymers onto nanoparticles to form a responsive corona offers potential in a wide range of technological, biological and medical applications where the interfacial properties are being modulated. This includes reducing non-specific protein binding, improving biocompatibility, preventing coagulation/aggregation, enabling sensing capabilities or modulating solubility. Hairy particles are one of the most widely used morphologies, due to their applications in drug release, catalyst supports, smart particulate emulsifiers, foam and liquid marble stabilizers, etc.

When grafting polymer chains onto the nanoparticle, the density onto the particle would have an impact on the cloud point of the polymer, which shows the same result compared to the film morphology. It has also been reported that the particle size would also effect on the transition temperature, this can be explained by the reason that the

density of the polymer is dependent on the degree of curvature. Figure 1.9[14] show the schematically curvature dependent polymer chain density, under the assumption that the chain is homogeneously grafted onto the nanoparticle.

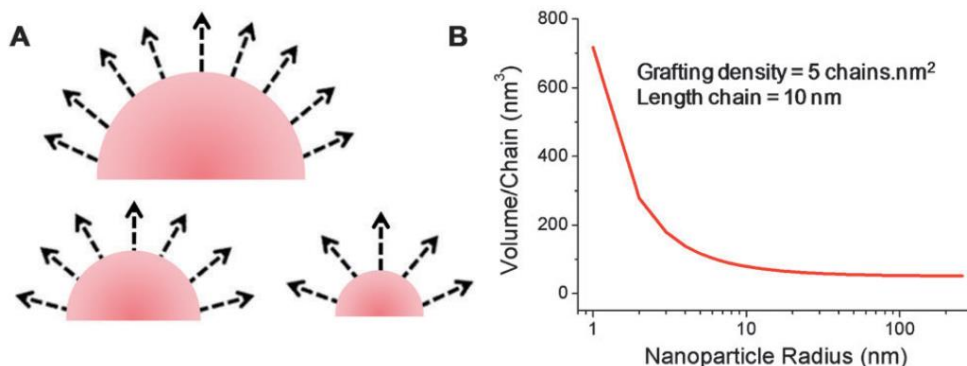


Figure 1.9. (A) Polymer chains grafted onto the nanoparticle with different diameter. (B) Calculated volume/chain as a function of nanoparticle radius. This picture is reprinted from Ref 14.

1.2.4.3 Other morphologies

Besides particle and film, many other morphologies are also widely investigated, like polymer brush layers, core-shell nanoparticles, capsules, lipid layers, hydrogels, capsule and micelle, etc. Versatile morphologies provide more possibility to investigate the stimuli-responsive polymers using different characterization methods such as atomic force microscopy (AFM), quartz crystal micro-balance (QCM), contact angle (CA) measurements, nanomechanical cantilever sensors, and so on.[30-32] Figure 1.10[5] displays the main morphologies used. Contributing to the versatile morphologies stimuli-responsive polymer can be used for many diverse applications, including drug delivery[33], smart biointerfaces[34], sensors[35], self-healing coatings[36], tunable catalysis[37], etc. For example, Nagasaki's team prepared nanogels, which are composed of a crosslinked, pH-sensitive polyamine core and conjugated PEO chains surround. These nanogels can be taken by cells through receptor-mediated endocytic

pathways. In the acidic endosome, the nanoparticles swell and release drugs reserved in the particle core.[38]

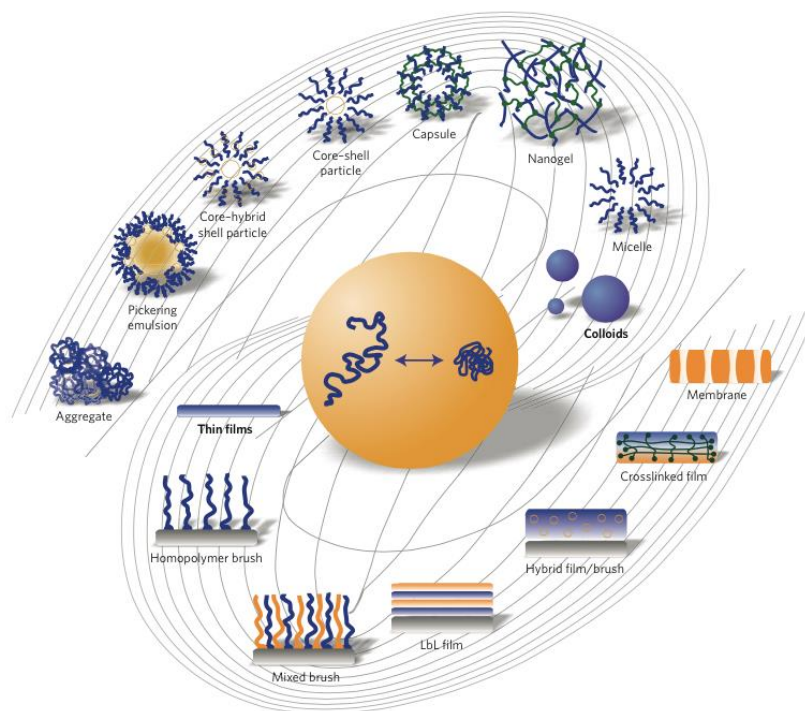


Figure 1.10. ‘Galaxy’ of nanostructured stimuli-responsive polymer materials. This picture is reprinted from Ref 5.

1.3 Motivation

Nowadays controlling the diffusion of penetrants in solution and nanostructured environments becomes a hot topic in colloid and polymer science. For this purpose different characterization methods are developed to study the diffusion, such as forces Rayleigh scattering (FRS)[39], fluorescence recovery after photobleaching (FRAP)[40], pulse-field-gradient NMR (PFG-NMR)[41], dynamic light scattering (DLS)[42], quasi-elastic neutron scattering (QENS)[43], etc. All these techniques have their own advantages and also some limitations. Generally they require high concentration of the diffusants in order to get high signal to noise ratio, but the high concentrations may

restrict the free diffusion behavior. Moreover, some specific task could be hard to realize with a given technique. Take DLS for example, the polarizability determines the extent of scattering and varies weakly with molecular structure, so DLS is not useful for measuring the progress of chemical reactions or for following the motion of a specific type of molecule at high dilution.

The theme of this thesis is to explore ways to control the diffusion (mobility) not only in solution but also in nanostructured environment. Stimuli-responsive polymers are ideal materials to construct the responsive species or the responsive environment for mobility control. As stimuli-responsive polymers show instant response under external stimuli, this would also bring the instant mobility change, thus an accurate and quantitative monitoring of the species is required to record the changing process. In this respect, fluorescence correlation spectroscopy (FCS) that is a powerful technique for studying the dynamics of fluorescent species in various environments offers an interesting alternative.[44] The fluorescent intensity fluctuations caused by the diffusion of the species through a very small confocal detection volume are recorded and the change process can be recorded. Because of its extremely small detection volume ($V < 10^{-15}$ L), high sensitivity is reached and even single molecule can be traced in the solution. Up until now, FCS has also found many applications in polymer and colloid science.[45-47] Furthermore, the method was applied to investigate stimuli-responsive polymer systems. For example, the pH or salt concentration induced changes in the size of individual polymer chains[48, 49], or in the interaction between small molecules and grafted polyelectrolyte brushes[50, 51], as well as, the temperature responsiveness of Poly(*N*-isopropylacrylamide) (PNIPAM) microgel particles[52], and grafted hydrogel films[53, 54] were studied.

In my thesis, I describe two approaches of using stimuli-responsive polymers to control the diffusion behavior, as exhaustively described in chapter 3 and 4. In both cases I used FCS as a technique to monitor and quantify the diffusion processes. The basics of the FCS techniques are discussed in chapter 2.

CHAPTER 2

Methods

2.1 Principle of fluorescence correlation spectroscopy (FCS)

Fluorescence correlation spectroscopy (FCS) is a powerful technique for studying the dynamics of fluorescent species such as small molecules, macromolecules, or nanoparticles in various environments.[55] In an FCS experiment the fluorescent light originating from a small probing volume formed around focused laser beam is detected. When a fluorophore diffuses into this volume fluorescent photons are emitted and detected due to multiple excitation-emission cycles from the fluorophore. When the fluorophore diffuses out of the volume the emitted photons disappear. In this way the diffusion of fluorophores causes time-dependent fluctuations in the detected fluorescence intensity. By correlation analysis of these fluctuations, one can determine the diffusion coefficient of the fluorophores. The time-dependent intensity fluctuations can be induced not only from translational or rotational diffusion, but also from photo-physical processes or chemical reactions that change the quantum efficiency of the fluorophores. Thus, FCS can be also used for studying such processes.

The FCS technique was first introduced by Madge, Elson and Webb in 1972[56, 57], who applied it to measure diffusion and chemical kinetics of DNA- Ethidium bromide (EtBr) intercalation. However, because of low detection efficiency, large probing volume (\sim nL) results in large ensemble numbers and insufficient background suppression, these early measurements show poor signal-to-noise ratios. Later, Rigler and his coworkers[58] made a breakthrough by combining the FCS technique with confocal detection that reduced the probing volume to \sim fL. This combined with the use of very sensitive avalanche photodiode detectors made the measurements of single

molecule trace in bulk solution possible and pave the way for the wide application of the FCS. Figure 2.1 shows the typical modern FCS setup[59]. In order that only the few fluorophores within the illuminated region are excited, a pinhole is also introduced to block all light not coming from the focal region, which limits the detection volume also in axial direction.

The excitation light is reflected by a dichroic mirror and focused into the sample by a high numerical aperture objective (ideally $NA > 0.9$) to a diffraction limited spot. The emitted light is collected by the same objective and passes through the dichroic mirror. Here the dichroic mirror acts so that the emission wavelength can be passed through and the excitation wavelength will be reflected. After passing through an emission filter and a confocal pinhole, the emitted light is detected by an avalanche photodiode detector (APD). Moreover, the confocal pinhole blocks the out-of-focus fluorescence and only the fluorescence from diffusants in the confocal observation volume can be detected. The confocal observation volume can be well approximated [58] with a 3D Gaussian ellipsoid with radial and lateral dimensions of r_0 and z_0 respectively.

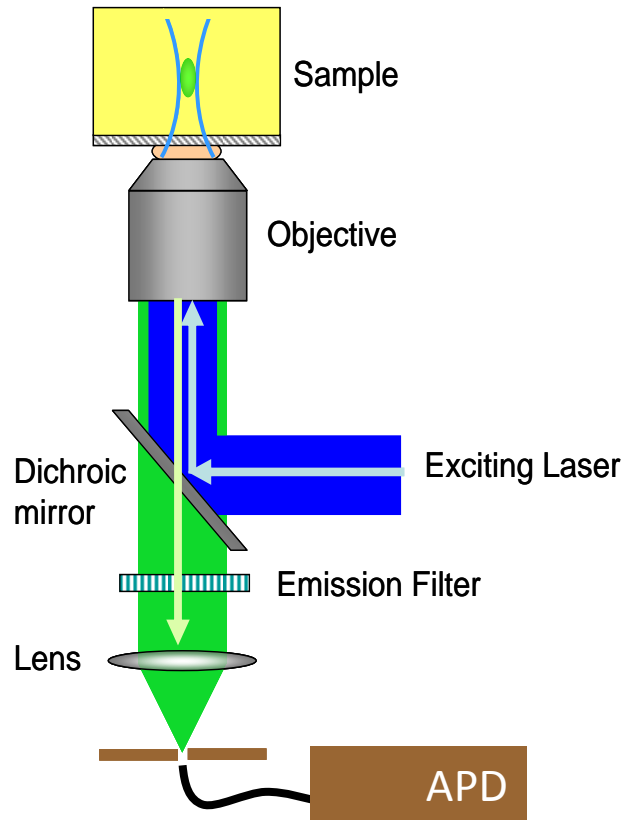


Figure 2.1. Scheme of a fluorescence correlation spectroscopy (FCS) setup.[59]

Here, I introduce the theoretical concepts how FCS works. As the fluorescent species diffuses through the confocal observation volume, the fluorescence fluctuations are produced, as shown in Figure 2.2[59]

$$\delta F(t) = F(t) - \langle F(t) \rangle \quad (2.1)$$

$\langle F \rangle$ is the average intensity. The normalized autocorrelation function is defined as

$$G(\tau) = \frac{\langle \delta F(t) \delta F(t+\tau) \rangle}{\langle F(t) \rangle^2} \quad (2.2)$$

In the simplest case when the intensity fluctuations are caused only by the diffusion of identical fluorescence molecules, the autocorrelation function describes the probability that a fluorescent molecule that was in the confocal volume V at time t will

be still there at time $t+\tau$. It can be shown [44] that in this case the autocorrelation function has following analytical form:

$$G(\tau) = 1 + \frac{1}{c \cdot V_{eff}} \frac{1}{\left(1 + \frac{4D\tau}{r_0^2}\right)} \frac{1}{\sqrt{1 + \frac{4D\tau}{z_0^2}}} \quad (2.3)$$

Here D is the diffusion coefficient of the fluorescent molecules and c – their molar concentration. V_{eff} is the effective confocal observation volume approximated by a three-dimensional Gaussian ellipsoid with radial and lateral dimensions of r_0 and z_0 so that

$$V_{eff} = \pi^{\frac{3}{2}} r_0^2 z_0 \quad (2.4)$$

As the typical values of r_0 and z_0 are roughly $0.2 \mu\text{m}$ and $1 \mu\text{m}$, respectively, we can calculate that the total volume is less than a $1\text{fL} = 10^{-15} \text{L}$.

Then we consider the relationship between the lateral diffusion time τ_D that a molecule stays in the confocal volume, and the diffusion coefficient D , which is independent of the particular setup used

$$D = \frac{r_0^2}{4\tau_D} \quad (2.5)$$

If we insert the Equation 2.5 and $N=c \cdot V_{eff}$ to the autocorrelation function $G(\tau)$, we get:

$$G(\tau) = 1 + \frac{1}{N} \frac{1}{\left(1 + \frac{\tau}{\tau_D}\right)} \frac{1}{\sqrt{1 + \frac{\tau}{S^2\tau_D}}} \quad (2.6)$$

Here, $S = z_0/r_0$ is the so-called structure parameter of the confocal volume. The diffusion coefficient D is related to the size of the fluorescent molecules via the Stokes-Einstein equation:

$$D = \frac{kT}{6\pi\eta R_H} \quad (2.7)$$

Where k is the Boltzmann constant, T is the absolute temperature, η is the viscosity of the medium and R_H is the hydrodynamic radius of the molecule.

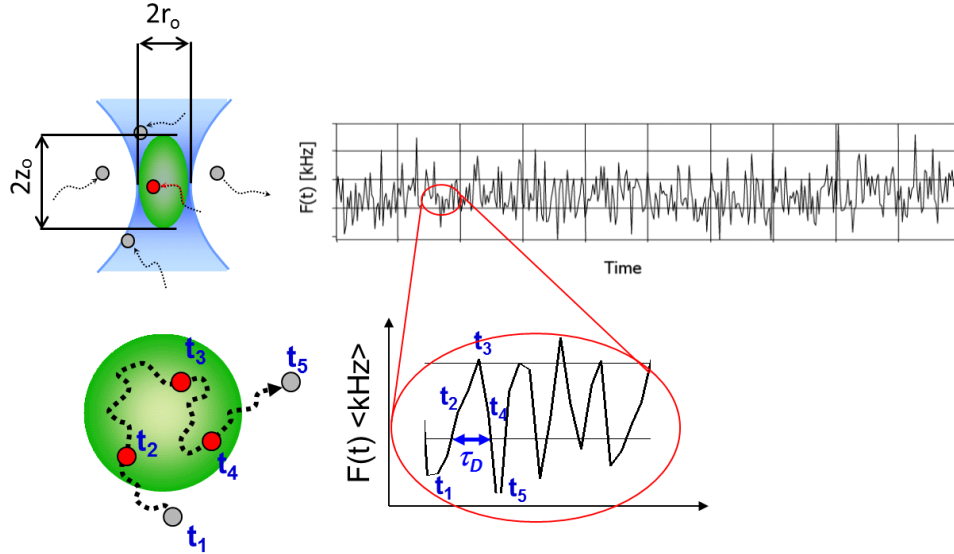


Figure 2.2. Fluorescence fluctuations caused by diffusing fluorescent species coming in and out of the observation volume.[59]

2.2 FCS experimental setup

The FCS measurements described in my thesis were performed on a commercial setup (Carl Zeiss, Germany) consisting of the modules LSM510, ConfoCor 2 and an inverted microscope model Axiovert 200 with a C-Apochromat 40 \times , NA 1.2 water immersion objective. Depending on the studied fluorophores the excitation was done either with an argon laser (488 nm) combined with a LP505 long pass emission filter or with a HeNe laser (633 nm) combined with a LP650 long pass filter. For detection an avalanche photodiode operating in single photon counting mode was used. Aqueous dispersions and solutions were studied either in 8-well, polystyrene chambered cover glass (Laboratory-Tek, Nalge Nunc International) or in an Attofluor cell chamber (Life Technologies) in which a microscope cover glass supporting the inverse opal structure

was mounted. For each studied sample series of 15 measurements with a total duration 5 min were performed. The experimental autocorrelation function was obtained by single photon counting, followed by binning and correlating using the commercial (Carl Zeiss) software correlator of the setup. The recorded experimental autocorrelation functions were fitted using the system software (Carl Zeiss) with the following analytical function:

$$G(\tau) = 1 + \left[1 + \frac{f_T}{1 - f_T} e^{-t/\tau_T} \right] \frac{1}{N} \frac{1}{\left[1 + \frac{\tau}{\tau_D} \right] \sqrt{1 + \frac{\tau}{S^2 \tau_D}}} \quad (2.8)$$

Here, the first term represent the so called triplet state dynamics and, f_T and τ_T are the fraction and the decay time of the triplet state, of the species, and S is the so-called structure parameter, $S = z_0/r_0$. The fits yielded the diffusion time τ_D and through Equation 2.5 the diffusion coefficient D of the studied fluorescent species. Next, the hydrodynamic radius R_H was calculated (assuming freely diffusing spherical particles) using Equation 2.7 $R_H = k_B T / 6\pi\eta D$. Furthermore, the molar concentration $c = N \cdot V_{eff}$ of the studied species and their molecular (or particle) fluorescent brightness $\langle F(t) \rangle / N$ were also determined. As the dimensions r_0 and z_0 of the confocal observation volume are not known a priori they were determined by performing calibration experiments using a fluorophore with known diffusion coefficient, e.g. Alexa 488 and 647 in water[60].

2.3 Scanning electron microscopy

The silica inverse opal structure was characterized by scanning electron microscopy (SEM) using a LEO Gemini 1530 microscope, at a voltage of 0.7 kV. For the cross section images of inverse opal, the substrate is with 75° tilt angle to the parallel.

2.4 pH meter

The pH value of the studied solutions was measured by a Seven Excellence pH meter from Mettler Toledo. Before pH measurement, pH meter was calibrated. Each pH value in my thesis was obtained by averaging three independent measurements.

2.4.1 pH adjustment

pH was adjusted by adding HCl and NaOH solution for the PDEA/PS hairy nanoparticle and PDEA single chain dispersion, and also in the confined environment. In PNIPAM modified inverse opal project, buffer solution was used. For Alexa Fluor 647, HPCE buffer solution (pH 8.0) from Sigma Aldrich is directly used; for the QD 525 with amino group, citrate buffer (pH 4.0) from Sigma Aldrich is directly used.

2.5 Gel permeation chromatography

Gel permeation chromatography (GPC) was used to determine molecular weight of the polymer obtained from bulk polymerization, which is believed to be comparable to the molecular weight of the chains grafted from surface. For GPC, PS was used as a standard; DMF was used as an eluent.

2.6. Materials

2.6.1 Fluorescent dyes

Fluorescent dyes are defined also as fluorescent molecules or fluorochromes. In 1933, Polish scientist Jablonski[61] publish one paper discussing how fluorescence is produced, as shown in Figure 2.3. The electrons in fluorescent dyes are normally in the ground singlet state. As fluorescent dyes adsorbs matched photon from outside, the

electrons can be excited to higher singlet state and return back to the ground singlet state, at the same time energy would release as fluorescent emission. The adsorption process last 10^{-15} s, which can be neglected as it occurs much faster than other transitions; the fluorescent emission process has the interval of 10^{-9} - 10^{-12} s. For these two processes we regard them as simultaneously happen. As there would be unavoidable energy loss like heat, the photon released would have a longer wavelength compared to the one adsorbed by the fluorescent molecules, so fluorescent dye adsorb one photon with higher energy and emit one photon with lower energy. But it can be also possible that the excited electron enter excited triplet state and then returns to ground singlet state, at the same time energy would release as phosphorescence. This process has interval of 10^2 - 10^{-2} s. As we can see that the lifetime of phosphorescence is quite long and phosphorescence quantum yield from the triplet state is very low, it is regarded as no luminescence. For qualified fluorescent dyes for FCS, high fluorescence efficiency and low triplet fraction are required. In practical application of fluorescent dyes, the environment would have also an important impact on the fluorescence efficiency, as triplet-state is dependent on the illumination intensity, concentration of molecular oxygen and some heavy metals or halogen ions. So for FCS measurements, we should choose fluorescent dyes with the high quantum efficiency, large absorption section and photostability.

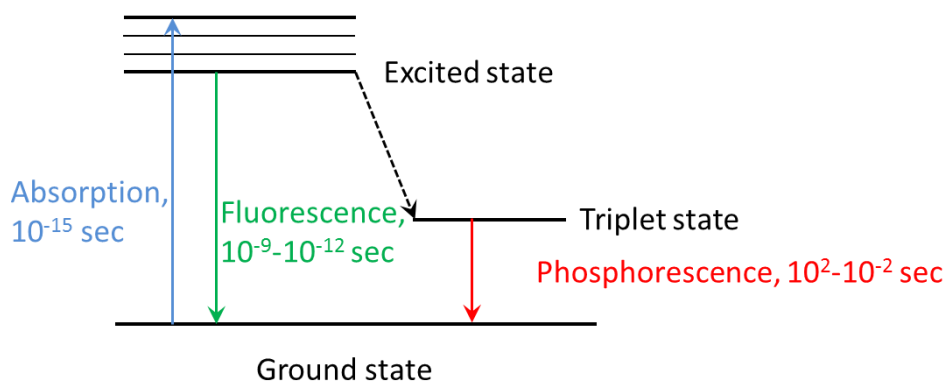


Figure 2.3. Jablonski diagram schematic illustration the generation process of fluoresce and phosphorescence.

2.6.1.1 Alexa series

Alexa Fluor dyes are synthesized through sulfonation of coumarin, rhodamine, xanthene (such as fluorescein), and cyanine dyes. Sulfonation makes Alexa Fluor dyes negatively charged and hydrophilic. Usually Alexa series are the most commonly used dyes as they own less pH sensitivity, photo stability and bright comparisons. Moreover, the excitation and emission spectra of the Alexa Fluor series cover the visible spectrum and extend into the infrared, which broaden its application area. Alexa series is a suitable candidate for FCS measurement. Fig 2.4a shows the structure of Alexa 488 and 2.4b is its adsorption and fluorescence spectra[62], 2.4c shows the structure of Alexa 647 and 2.4d is its adsorption and fluorescence spectra[63].

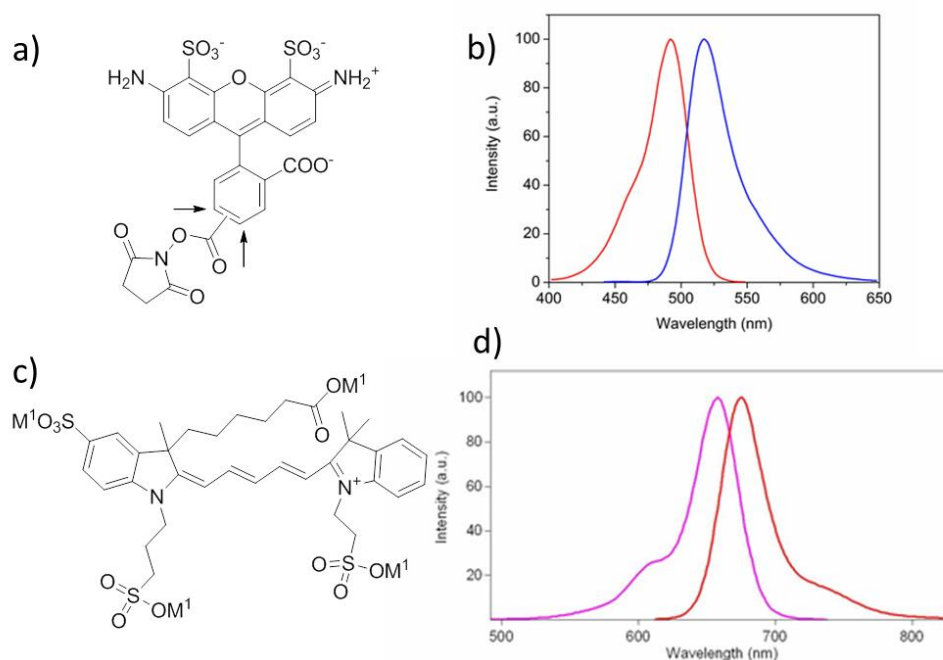


Figure 2.4. (a) Molecular structure of Alexa 488 and (b) its absorption and fluorescent emission spectra[62]; (c) Molecular structure of Alexa 647 and (d) its absorption and fluorescent emission spectra[63].

2.6.1.2 Bodipy

Bodipy is the abbreviation of boron-dipyrromethene, which is a kind of fluorescent dyes. Bodipy is composed of dipyrromethene complexed and a disubstituted boron atom, typically a BF_2 unit. The core part is 4,4-difluoro-4-bora-3a,4a-diaza-s-indacene (Figure 2.5a) and normally it is decorated with other functional group for different use.[64] Bodipy is a bright, green-fluorescent dye with similar excitation and emission to fluorescein or Alexa Fluor. It has a high extinction coefficient and fluorescence quantum yield and is relatively insensitive to solvent polarity and pH change, in addition it can't be dissolved in water solution, so it's an ideal dye for the pH-responsive system. Figure 2.5b is the molecular structure of 4,4-difluoro-5,7-dimethyl-4-bora-3a,4a-diaza-s-Indacene-3-propionic acid, succinimidyl ester from Life Technologies we are using in this thesis, and Figure 2.5c shows its absorption and fluorescent emission spectra[65].

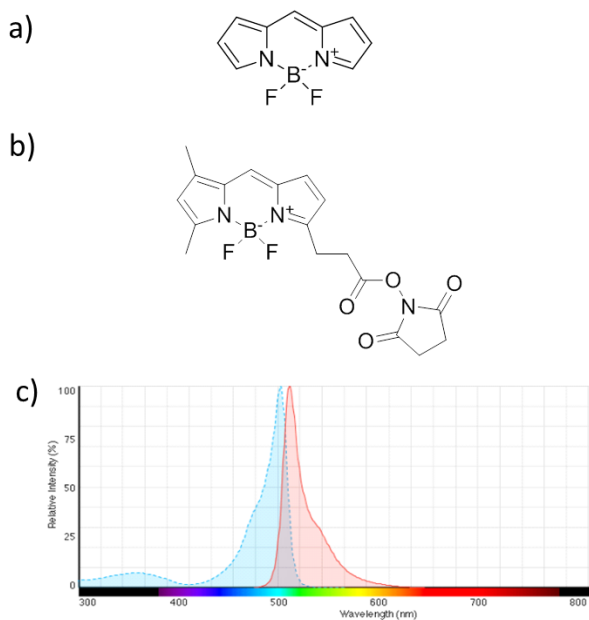


Figure 2.5. (a) Molecular structure of Bodipy core, (b) Molecular structure of Bodipy used in this thesis and (c) its absorption and fluorescent emission spectra[65].

2.6.1.3 Quantum dots

Quantum dots (QDs) are nanocrystals made of semiconductor materials that are small enough to exhibit quantum mechanical properties.[66] QDs are nanometer-scale atom clusters composing of cadmium mixed with selenium or tellurium, ranging from a few hundred to a few thousand atoms, moreover an additional semiconductor shell like zinc sulfide is coated to improve the optical properties of the material. Furthermore, polymers coating can be also coated to adjust the solubility in solvent or conjugate QDs to biomolecules. Electronic characteristics of a quantum dot are closely related to its size and shape. One important character of QDs is the frequency range of emitted light is highly dependent on its size-the frequency of emitted light decreases as the size of the quantum dot increases, so the emission of QDs can be well controlled during the synthesis process.[67] Figure 2.6a shows how the size of QDs determines the fluorescent color[68] and Figure 2.6b and c shows the absorption and emission spectra of four CdSe/ZnS qdot samples[69].

Quantum dots own a long-term photostability, brilliant colors and narrow, symmetrical emission spectra, which make them also good candidates as a tracer. Moreover, its size is bigger than the Alexa series and Bodipy, and this broaden the size range of the dye and also the responsive range as the surrounding environments changes. With different end group the QDs behaves differently in solution, and the pH in solution would also have an impact on the stability of QDs. I use QD525 with amine-derivatized poly ethyl glycol (PEG) in my thesis; with the PEG chain non-specific interactions can be avoided.

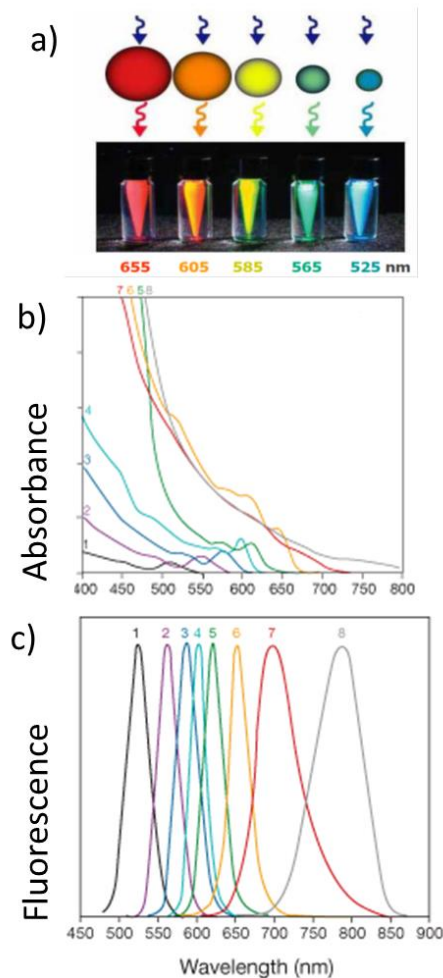


Figure 2.6. (a) Five different nanocrystal solutions excited with the same long-wavelength UV lamp.[68] (b) Absorption and (c) emission spectra of four CdSe/ZnS qdot samples.[69].

2.6.2 Silica inverse opals

Silica inverse opal is a three-dimensional ordered structure which is consisting of regular spherical voids with interconnecting circular pores, and the silica wall made it with good mechanical stability.

2.6.2.1 Silica and PS nanoparticles

Silica was purchased from Sigma Aldrich with 30% concentration and diameter of 7 nm and used as received; PS nanoparticle (1 μm , 330 nm and 200 nm in diameter) were synthesized according to the literature.[70] Round microscope glass slides with diameter of 25 mm and thickness of 170 μm , were purchased from Menzel, Germany and cleaned with a 2% Hellmanex solution (Hellma, Germany) prior to further use.

2.6.2.2 Preparation

Inverse opals structures on a thin glass slide substrate were prepared as described in details elsewhere.[71-74] Briefly the substrate was lifted with 400 nm/s lifting speed from a mixed aqueous dispersion of 1.5 wt% PS particles and 0.3 wt% silica nanoparticles at 20 °C environmental temperature and 50% RH environmental humidity as measured. As we only want one side of the substrate is coated with inverse opal structure, the opposite side is coated with polyethylene film which blocks the contact of mixture dispersions and the substrate. Schematic illustration of the fabricating process is shown in Figure 2.7.

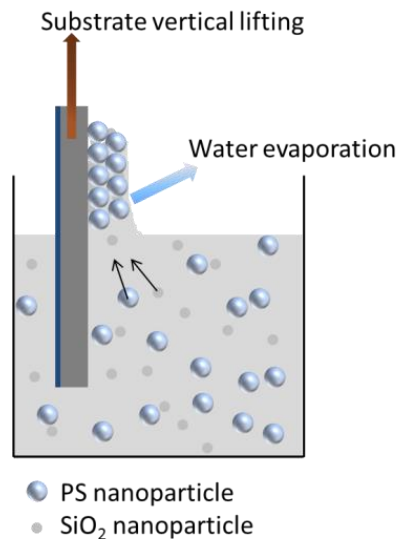


Figure 2.7. Scheme of the vertical lifting deposition of mixture dispersions of PS nanoparticle and SiO₂ nanoparticles.

The polyethylene film on the other side of the substrate is peeled off before high temperature calcination. The PS template was removed by pyrolysis in air at 500 °C for 5 hours, leaving the silica nanoparticle stacked and fused in an ordered three-dimensional structure, shown in Figure 2.8.

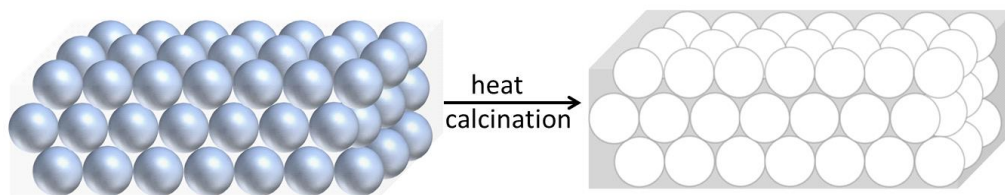


Figure 2.8. Preparation of silica inverse opal by high temperature calcination.

Following this method, we can get ordered three-dimensional inverse opal structure. Figure 2.9 show the SEM images from top view and side view of silica

inverse opal made from dispersions of silica nanoparticle and PS nanoparticle with diameter of 200 nm, 300 nm and 1 μm , respectively.

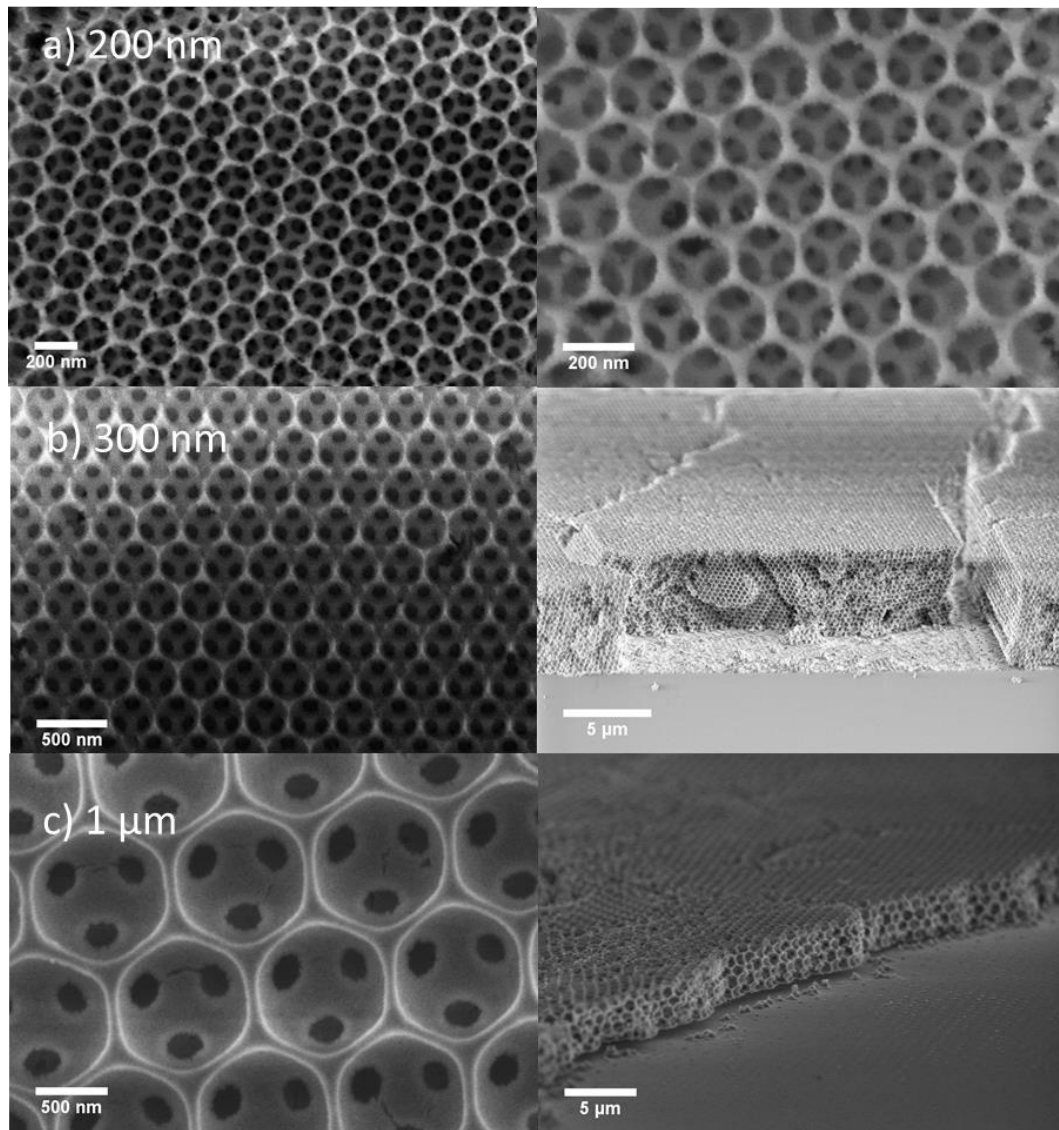


Figure 2.9. Scanning electron microscopy images of inverse opals made from (a) 200 nm, (b) 300 nm, (c) 1 μm polystyrene particles in diameter.

2.6.3 PS/PDEA hairy nanoparticles and PDEA single chains

... provides us the PS/PDEA hairy nanoparticle and PDEA single chain. To enable the fluorescence, the BodipyBODIPY is covalently bounded to the PS/PDEA hairy nanoparticle and PDEA chain. Detailed synthesis processes are described in our paper.[75]

2.6.4 Cells for FCS measurement

For the FCS measurements in solution, 8-well chambers from Nunc Lab-Tek were used. For the FCS measurement in the inverse opals, an Attofluor cell chamber (Invitrogen, Leiden, Holland) was used as a sample cell, in which one glass slide with 25 mm in diameter and 170 μm in thickness is mounted, and the diluted dye solution is deposited on top to cover the inverse opal coated glass slide totally, on top of the whole cell another clean glass slide is added to prevent the water vapor condensed at the detection camera lens. Figure 2.10 show 8-well chamber (a)[76] and the Attofluor cell chamber (b)[77]. To study the temperature dependence of nanoparticle mobility by FCS, an extra commercial heating setup is added, which is shown in Figure 2.10c.

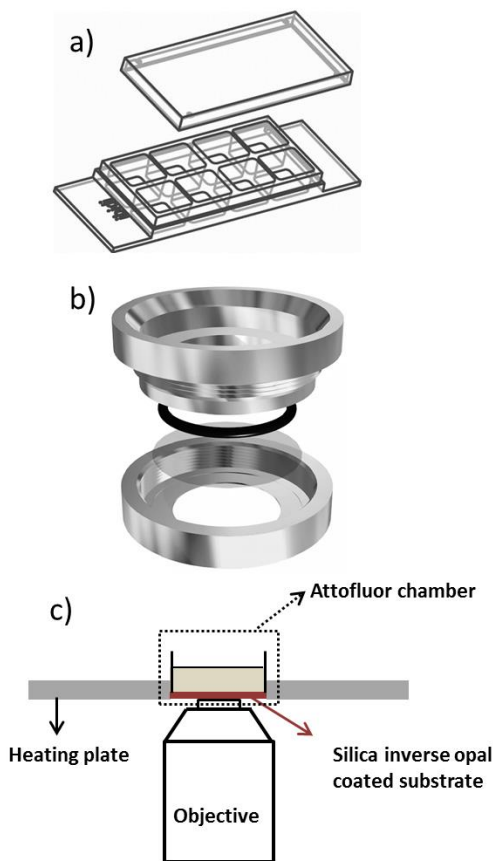


Figure 2.10. (a) 8-well chamber[76]. (b) Attofluor cell chamber[77] and (c) Scheme of the heating setup.

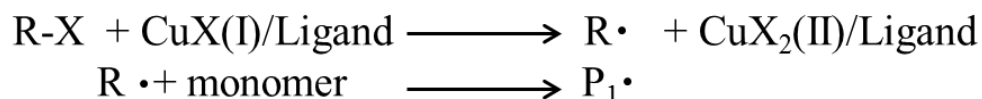
2.7 Atom transfer radical polymerization (ATRP)

Free radical polymerization is one kind of polymerization methods by continually adding free radical building block to form polymer. Because it requires relatively non-specific nature of free radical chemical interactions, it becomes one of the most versatile methods to obtain a wide variety of different polymers and materials composite. Among the radical polymerizations, reversible deactivation radical polymerization are the most popular used, which includes atom transfer radical polymerization (ATRP), reversible addition-fragmentation chain transfer polymerization

(RAFT) and stable free radical polymerization (SFRP).[78, 79] Among these methods ATRP are well used for surface initiated polymerization. Here, I would take ATRP for example to introduce the mechanism and the polymerization condition.

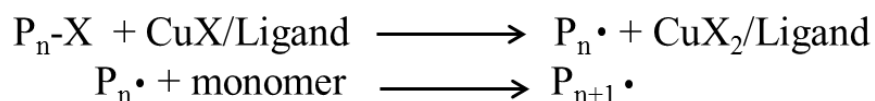
ATRP was independently discovered by Mitsuo Sawamoto [80] and Jin-Shan Wang and K. Matyjaszewski [81, 82] in 1995. ATRP is controlled by equilibrium between propagating radical and dormant species.[83] For ATRP, it can be divided into three steps: initiation stage, propagation stage and end stage.[84]

Initiation stage:



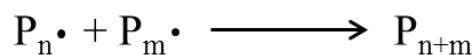
R-X is alkyl halides, which is used as the initiator, CuX is on behalf of redox-active transition metal complexes; ligand, whose electronic effect and steric effect would have an important impact on the activation and deactivation activity of the catalyst. Cu(I) is the activator, R• is the radical, CuX(II) is the deactivator, P• is the growing radical.

Propagation stage:



P_n-X is activated by CuX/ligand to become radical, and more monomers can be grown on the active radical to get large molecular weight.

Termination stage:



Two radical grow together to terminate the polymerization.

In order to analyze the mechanism of ATRP, a more general scheme can be got (Figure 2.11),

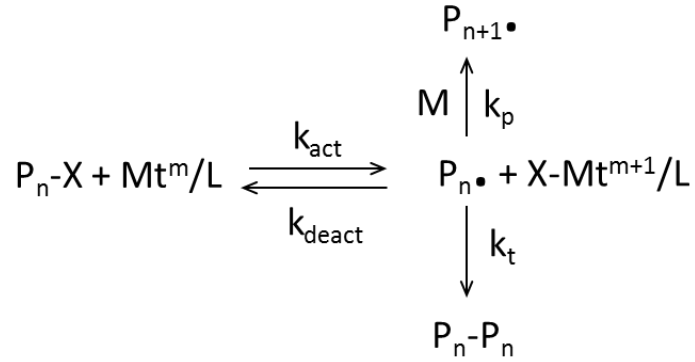


Figure 2.11. Scheme of the ATRP mechanism.

P_n-X is the dormant species, which is normally alkyl halides/macromolecular species; Mt^m/L is activators, in which Mt^m represents the transition metal species in oxidation state m , L is ligand; P_n is the growing radicals, $X-Mt^{m+1}/L$ is the higher oxidation state. For simplification, I use copper-mediated ATRP for example, so C_u^I and C_u^{II} represent Mt^m and Mt^{m+1} , respectively. k_p is rate constant of the propagation; k_{ATRP} is the ratio of k_{act} (the rate constant of activation) and k_{deact} (the rate constant of deactivation), which determinate the polymerization rate; k_t is the rate coefficient of termination.

According to the propagation of generated radicals, we can get:

$$R_p = k_p [M][P_n \bullet] \quad (2.9)$$

In addition, we can get the $[P_n \bullet]$ according to the whole equilibrium:

$$[P_n \bullet] = k_{ATRP} \frac{[P_n X][C_u^I/L]}{[XC_u^{II}/L]} \quad (2.10)$$

Insert Equation 2.10 to 2.9, we can get:

$$R_p = k_p [M][P_n \bullet] = k_p k_{ATRP} \frac{[P_n X][C_u^I/L][M]}{[XC_u^{II}/L]} \quad (2.11)$$

From Equation 2.11 we could see that R_p depends on the catalyst activity (K_{ATRP}), concentration of monomer, the redox-active transition metal complexes. Moreover, ligand species, monomer/dormant species, and the reaction condition (solvent, temperature, pressure, etc.) would also have an impact on the polymerization rate. Once the initiator is added, all the monomer can be immediately activated, and the chain can grow at the same time, so the low molecular weight polydispersity can be got. If the transfer and termination are negligible, the degree of polymerization can be calculated:

$$X = \frac{[M_0]}{[I_0]} \quad (2.12)$$

$[M_0]$ is the monomer concentration, $[I_0]$ is the initiator concentration. But we need to pay attention that during the polymerization process, the generated radicals can react not only with monomer but also with other generated radicals, which means that the termination occurs at the same time. Here we need to compare k_p and k_t . As k_{deact} is much larger than k_{act} , for most of the monomer are in the dormant species, and the concentration of radical is low, the generated oxidized metal complexes, $X-Mt^{m+1}/L$ acts at persistent radicals to reduce the stationary concentration of growing radicals and minimize the concentration of termination. Typically in a well-controlled ATRP, people can get a small amount of terminated chains but a uniform growth of all the chains with low molecular weight polydispersity ($PD = \frac{W_m}{W_n}$) which is proximately between 1.0 and 1.5.

In the past years, different designed morphologies can be polymerized by ATRP, like linear chains, block copolymers, cyclic structures, etc. Moreover, the dimensions and dispersity can be also well controlled.[83] Figure 2.12 shows controlled topology prepared by ATRP. As it provides a simple route for many well-defined (co)polymers

with predetermined molecular weight, narrow molecular weight distribution, and high degree of chain end functionality, which broaden the substance field of stimuli-responsive polymer in nature.

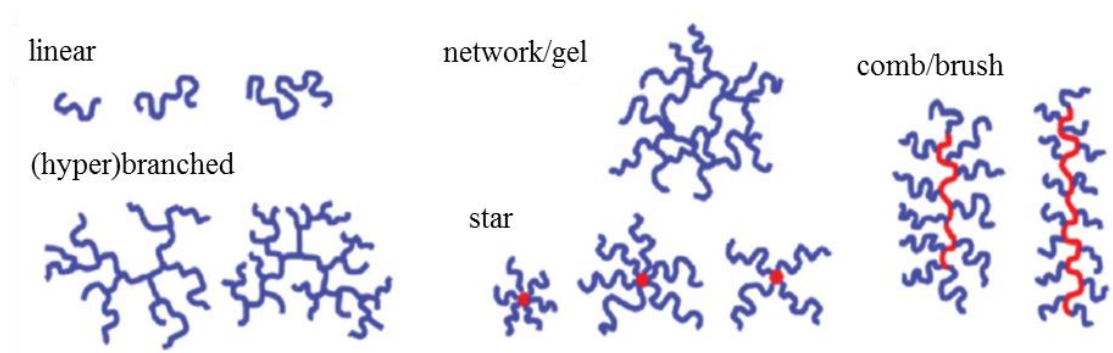


Figure 2.12. Polymers with controlled topology prepared by ATRP, reprinted from Ref 76.

2.7.1 “Grafting from”

In general, the ATRP technique includes “grafting from” and “grafting to” techniques. For the “grafting from” technique, firstly the initiators are fixed on the substrate, then monomer propagates onto it and the polymer chains grow (Figure 2.13). As the initiators can be fixed tightly by chemical reaction and monomer can diffuse freely in the solution to the growing chain, high density of polymer brushes and low poly dispersity can be obtained.

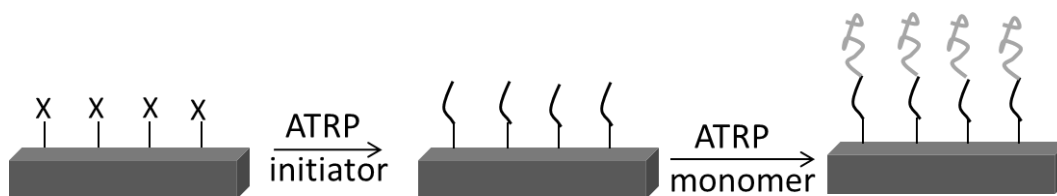


Figure 2.13. Graft of polymers from an initiator-functionalized substrate.

For the “grafting from” technique, the initiator groups can be successfully coated onto both organic and inorganic materials, both flat and curved surfaces. As a

consequence, polymer brushes of varying composition and dimensions can be prepared by surface-initiated growth from like on spheres, flat solid surface or colloids.[85]

2.7.2 “Grafting to”

The “grafting to” technique is also a widely used technique in ATRP. Usually the monomers polymerize to the polymer chains in solution, and then the whole polymer chains are grafted onto the substrate decorated with initiators. Compared to the “grafting from” technique, “grafting to” leads to lower brush densities as it is limited intrinsically by the excluded volume effects. As polymer brushes are sterically less confined when they are prepared by the grafting to technique, it would broaden the cloud point transition compared to highly dense polymer brushes.

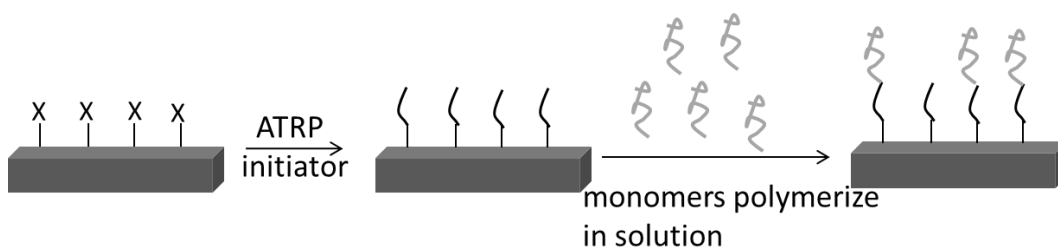


Figure 2.14. Graft of polymer chains onto preformed substrate.

CHAPTER 3

Temperature controlled diffusion in PNIPAM modified silica inverse opals

In this chapter, I report a new strategy for the preparation of well-defined and mechanically stable porous nanostructures with tunable porosity. Silica inverse opals, which are known as a model system for a porous periodic nanostructure, were grafted with brushes of the thermo-responsive poly(*N*-isopropylacrylamide) (PNIPAM) grown via atom transfer radical polymerization. By tuning the temperature I was able to control the overall porosity of the system and thus the mobility of small penetrants. Fluorescence correlation spectroscopy was used to directly monitor and *in situ* quantify the changes in the penetrants' mobility, which is caused by changes of polymers conformation.

3.1 Introduction and motivation

Understanding and controlling the diffusion of small molecules, macromolecules and nanoparticles in complex, nanostructured environments is of paramount fundamental and technological importance. Often, diffusion is the dominant mechanism for the transport of such species in e.g. solid nanoporous structures, polymer solutions and gels or in living cells. Thus, it is relevant for many processes and applications including drug delivery, cell nutrition, porous chromatography, polymer synthesis and separation, treatment of waste water, oil recovery, etc. Not surprisingly therefore, studying the penetrant diffusion and correlating it to the chemical, physical and topological characteristics of the nanostructured environment has become a major research topic in various fields spanning from polymer physics to cell biology. A number of theories, models and empirical relations have been introduced to describe the

diffusion of small species in polymer systems, in intercellular matrices or in solid periodic nanoporous structures.

From application point of view, the possibility for on demand control over the diffusion of small penetrants in nanoporous structures is even more important. Indeed, such possibility gives various opportunities as to e.g. control the drug release rate or to select the relevant sizes in a separation process. Traditionally, control over the penetrant diffusion is achieved by changing the size and/or density of the nanopores. However, in a solid nanoporous structure, such as an anodized aluminum membrane, a porous glass or a silica inverse opal, the pore size is determined during the fabrication process and typically cannot be changed e.g. by applying an external stimulus. This is unfortunate, as the solid nanoporous structures offer the mechanical strength and stability that is required for most applications. Alternatively, in some polymer based nanoporous systems such as e.g. hydrogels, the pore size and thus the penetrant diffusivity can be controlled by tuning the temperature or the pH value. Hydrogels, however, lack mechanical stability that often makes their application problematic.

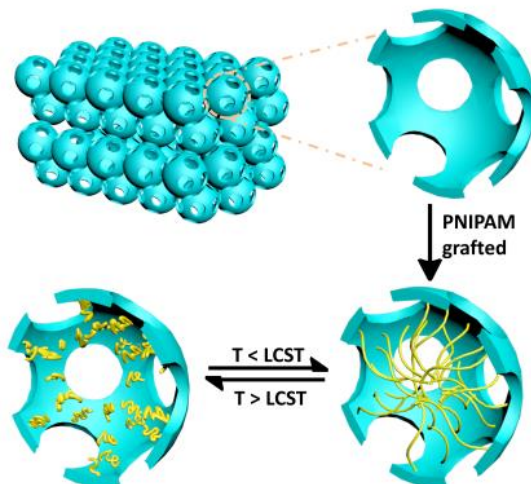
In this chapter, I describe a new system combining the mechanical stability of a solid nanoporous structure with the possibility for fine tuning offered by a thermo-responsive polymer. As a solid support I used a silica inverse opal (iOpal), which is a highly order porous structure, consisting of regular arrangements of spherical voids surrounded by solid silica walls with interconnecting circular pores.[71-74] Due to their well-defined nanoporous structure iOpals have been often used as model system to study the diffusion of small molecules[86], nanoparticles[87] or DNA[88]. Here, in order to add responsiveness and tunability to the nanoporous structure I modified the iOpal interior surface with grafted poly(*N*-isopropylacrylamide) (PNIPAM) brushes by surface initiated atom transfer radical polymerization (ATRP). The PNIPAM is one of the most popular thermo-responsive polymers and exhibits a lower critical solution temperature (LCST) of around 32 °C[15] i.e. close to the humans body temperature. In aqueous solutions, below the LCST the PNIPAM chains are hydrated and adopt an extended coil conformation, while above the LCST they are dehydrated and collapse to a globular

conformation. Correspondingly, the PNIPAM brushes grafted to the iOpal interior surface will swell under the LCST decreasing the overall porosity of the system and shrink above the LCST increasing the porosity. This offers the possibility for a temperature control over the diffusivity of small penetrants inside the iOpal. Correspondingly, the PNIPAM brushes grafted to the iOpal interior surface will swell under the LCST decreasing the overall porosity of the system and shrink above the LCST increasing the porosity. This offers the possibility for a temperature control over the diffusivity of small penetrants inside the iOpal.

PNIPAM, grafted on porous silica nanoparticles[89] or porous silicon films[90] were used previously for temperature controlled entrapping and release of model drug molecules. Here, I go a step further and focus on direct monitoring of the penetrants mobility inside the PNIPAM modified iOpal. For this purpose I used fluorescence correlation spectroscopy (FCS)[91] a method combining single molecule sensitivity with very small probing volume ($< 1 \mu\text{m}^3$) that can be easily positioned on various places in the studied nanoporous structure and thus provide local information on the penetrant mobility. While initially developed and still predominantly used in molecular and cell biology,[92] FCS has also found further widespread applications[45-47] and was employed to study dynamics in various polymer systems[52, 53, 93-104], interface[105], and solid porous structures[86, 87, 106, 107]. In particular the method was successfully used to investigate penetrants diffusion in both PNIPAM gels[52, 53, 97] and unmodified silica iOpal[86, 87].

I used FCS to investigate the diffusion of small fluorescent tracers in silica inverse opal modified with temperature responsive polymeric brushes and found that it is significantly slower than the diffusion in unmodified ones. Additionally, I demonstrate that it is indeed possible to control the penetrants diffusion via the stretching and collapsing of polymer brushes in this nano-engineered system by simply tuning the temperature. Scheme 3.1 shows the main process considered in this chapter. Firstly the silica inverse opal is prepared, and then PNIPAM brush is grafted onto the silica inverse opals by atom transfer radical polymerization. Later the changes in the

fluorescent species mobility caused by the different conformations of the PNIPAM chains are studied by FCS.



Scheme 3.1. Scheme of temperature controlled diffusion in PNIPAM modified silica inverse opals.

3.2 Atom transfer radical polymerization on silica inverse opals

3.2.1 Preparation of the silica inverse opals

The silica inverse opals with the void diameter of 315 nm were fabricated by vertical deposition (VD) method as described in Chapter 2. Typical scanning electron microscopy (SEM) images of as prepared inverse opals are shown in Figure 2.9 in Chapter 2. The inverse opal has a thickness of 5 microns with a void diameter and interconnecting circular pores size of 315 nm and 105 nm respectively. In addition some defects and cracks can be observed, which usually form during drying and calcination process.[108, 109] However such cracks can be easily seen in laser scanning confocal

microscopy (LCSM) and in order to avoid contributions of tracer diffusion in cracks all the FCS measurements were done in the center of continuous platelets (Fig 3.1).

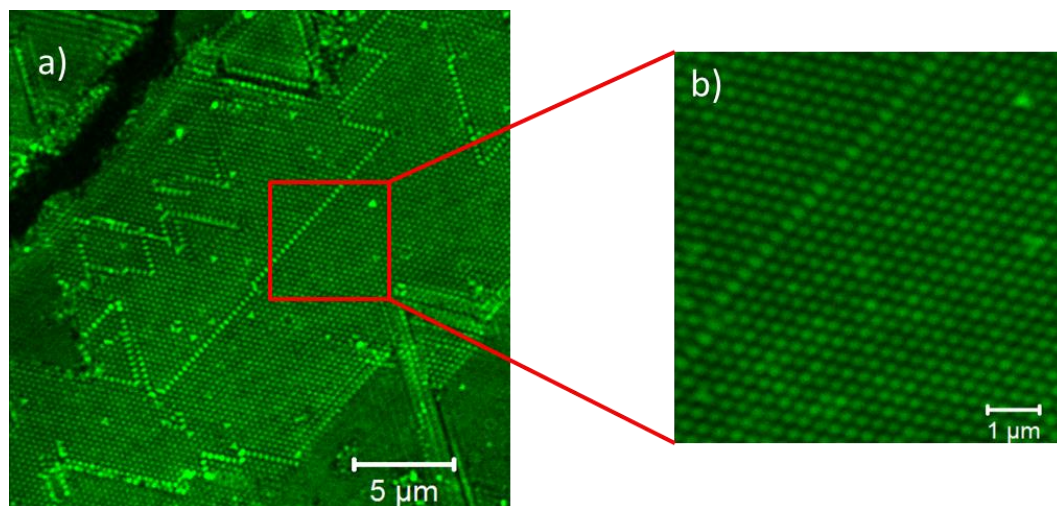


Figure 3.1. Reflectance images of silica inverse opal taken with the confocal microscope part of the FCS setup.

3.2.2 ATRP on silica inverse opals

Then the silica inverse opals were coated with PNIPAM chains using “grafting-from” technique in ATRP.

3.2.2.1 Materials

N-isopropylacrylamide (NIPAM), CuCl, H₂O₂ (35%), methyl (S)-2-chloropropionate, triethylamine (TEA) and anhydrous toluene were purchased from Aldrich. NH₃ (25%) was purchased from VWR Chemicals. Tris (2-dimethylaminoethyl) amine was purchased from Alfa Aesar. TEA was distilled from CaH₂, and the starter 3-(2-bromoisobutyryl)propyl)dimethyl chlorosilane was synthesized following the procedure described in the literature.[110] In order to prevent degradation by moisture,

the starter and TEA were both stored under argon atmosphere. NIPAM monomer was recrystallized from hexane. The precipitate was rinsed with water, ethanol, and finally with diethyl ether and dried in a vacuum oven for 24 h. Anhydrous toluene and tris (2-dimethylaminoethyl) amine were used directly after purchased. All aqueous solutions were prepared with ultrapure water purified with a Milli-Q UV-Plus water purification system (Millipore, Bedford, MA). The water had a resistivity of $>18 \text{ M}\Omega\text{cm}^{-1}$.

3.2.2.2 Initiator immobilization

In order to prepare the silicon surface for the starter immobilization and to assure controlled hydration state of the silicon oxide layer on top, a base cleaning was performed. Silica inverse opal was immersed in a mixture of NH_3 (4 mL, 25%), H_2O_2 (4 mL, 35%) and Millipore water (50 mL) for 2 hours at room temperature. Afterwards, the silicon surface was rinsed with abundant amounts of Millipore water and dried with a N_2 flow.

Then the freshly cleaned silica inverse opal was is immersed in mixed solution of 0.4 mL TEA, 0.2 mL 3-(chlorodimethylsilyl) propyl 2-bromo-2-methylpropanoate and 25 mL anhydrous toluene with stirring for 10 h under argon, and then wash with dichloromethane placed in soxhlet apparatus for 6 hours and used for graft polymerization.

3.2.2.3 Surface-initiated polymerizations

The surface-functionalized silicon substrate was placed in the tube and the reaction solution was prepared in DMF/ H_2O (1:1, $V = 28 \text{ mL}$) containing the monomer NIPAM ($m = 2.72 \text{ g}$), the ATRP catalyst CuCl ($m = 19 \text{ mg}$) the ligand tris (2-dimethylaminoethyl) amine ($V = 55.8 \mu\text{L}$) and sacrificial initiator $22 \mu\text{L}$ Methyl (S)-2-chloropropionate. The polymerization mixture was carefully degassed through several freeze-thaw cycles to remove dissolved oxygen and the polymerization was carried out

at room temperature. After 45 min reaction time the silica inverse opal was removed from the polymerization mixture rinsed with dichloromethane and dried.

Subsequently, the glass slides were placed in a Soxhlet apparatus, continuously extracted with methanol for 18 h, and dried under argon. The PNIPAM solid was obtained by dialyzing the PNIPAM solution with the 1000 g/mol dialysis tube for 3 days and then removing the solvent by one rotary evaporator, and GPC is used to determine the molecular weight of PNIPAM. The number-average molecular weight (M_n) is 21000 g/mol, as shown in Figure 3.2.

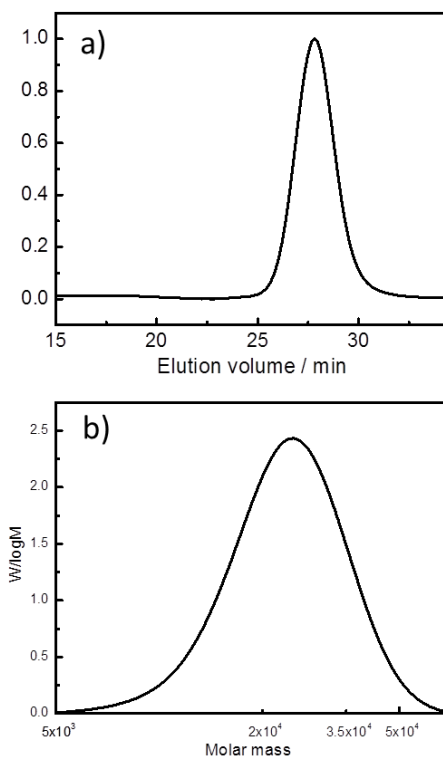


Figure 3.2. Gel-permeation chromatography results of the polymer with $M_n = 21000$ g/mol synthesized in solution. (a) Elugram of the PNIPAM chains. (b) Molecular weight distribution.

Modified inverse opals were also analyzed with SEM and compared to unmodified one (Figure 3.3). From SEM images we can see the presence of the polymer layer grafted on the surface of the inverse voids, resulting in the pores between interconnecting holes are getting smaller.

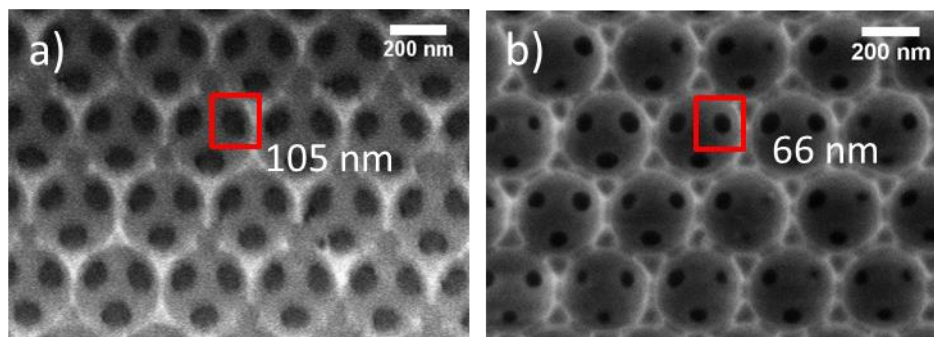


Figure 3.3. Inverse opals images before and after grafting PNIPAM chains.

Moreover, the optical image of inverse opal coated on the glass slide can also show that PNIPAM chains are successfully grafted onto the inverse opal. As shown in Figure 3.4, the color of the substrate is turning from green to red after being coated with PNIPAM chains. For the right image we see that there is a small piece of green color, this is because of it got in touch with the holder of the substrate which can't be exposed to the solution during the polymerization. These optical images are taken vertically from the top. This structure color can be explained by Bragg's law.[111]

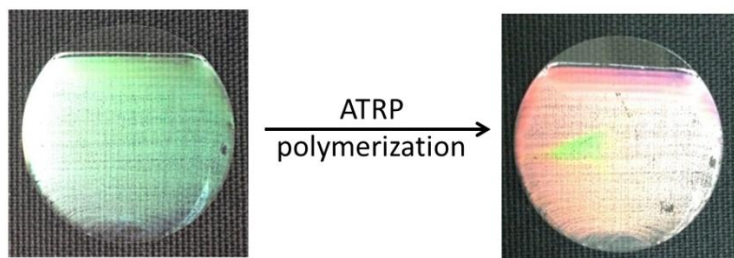


Figure 3.4. Optical images of silica inverse opal coated substrate before and after grafting PNIPAM chains.

3.3 Dyes and solvents for FCS measurement

Alexa Fluore 647 and QD 525 were purchased from Invitrogen (Karlsruhe, Germany) and used as tracers. For the FCS measurement solutions of either Alexa Fluore 647 with concentration ~ 5 nM in HPCE buffer (pH 8.0) or QD 525 with concentration 20 nM in citrate buffer (pH 4.0) were used.

3.4 Alexa 647 and QD 525 diffusion in PNIPAM grafted silica inverse opals

The FCS measurements were performed on a commercial setup (Carl Zeiss, Germany) consisting of the modules LSM510, ConfoCor 2 and an inverted microscope model Axiovert 200 with a C-Apochromat (40 \times , NA 1.2) water immersion objective. A HeNe laser (633 nm) was used for exciting Alexa 647, and the emission was collected after filtering with a LP650 long pass filter; an argon laser (488 nm) was used for exciting QD 525, and the emission was collected after filtering with a LP505 long pass filter. The fluorescent tracers solutions were studied either in 8-well, polystyrene chambered cover glass or in an Attofluor cell chamber in which a microscope cover glass supporting the inverse opal structure was mounted. Reflection mode imaging was performed with the same objective (C-Apochromat 40 \times), using excitation at very low intensity at the laser wavelength of 488 nm combined with a long pass LP 475 emission filter.

First, I used FCS to study the effect of the grafted PNIPAM brushes on the diffusion of the small molecular dye-Alexa Fluor 647 in the modified iOpal. It is important to emphasize that due to the extremely small probing volume of the FCS (~ 1 μm in axial direction) the small fluorescent tracer diffusion studies can nicely capture this gradient in film as thin as few micrometers only. Even though cracks are presented among iOpal, they can be clearly visualized by confocal microscopy in reflection mode,

which helps to define the exact location in the iOpal for tracer mobility measurements (Figure 3.1). In my experiments, the objective's immersion medium was water with refractive index $n \approx 1.33$. For the water-filled PNIPAM modified inverse opal with silica ($n \approx 1.45$) and filling volume fraction of about 20%, the effective refractive index was $n \approx 1.36$. Due to this small refractive index mismatch, the estimated error of the diffusion in the inverse opals was less than 10%. [73, 87, 112] Thus the strong shift of the autocorrelation curves for the inverse opal toward to longer times was caused by the confinement, as discussed and theoretically rationalized before. [87]

Figure 3.5 shows a typical FCS autocorrelation curve measured in the middle of an iOpal modified with PNIPAM with $M_n = 21000$ g/mol. The autocorrelation curves of Alexa 647 measured in the iOpal and iOpal modified with PNIPAM chains are strongly shifted to the longer lag times, reflecting significantly slower diffusion. Both curves can be nicely fitted with Equation 2.8 yielding diffusion times of $\tau_d = 75$ μ s and $\tau_d = 122$ μ s in the iOpal and in the iOpal modified with PNIPAM brushes, respectively. For comparison the diffusion of the same tracer in bulk citrate buffer solution is even faster with diffusion time $\tau_d = 56$ μ s (the circle solid line). In order to verify the reproducibility of these results, FCS measurements were performed at various lateral positions in the studied iOpal, which yielded very similar results.

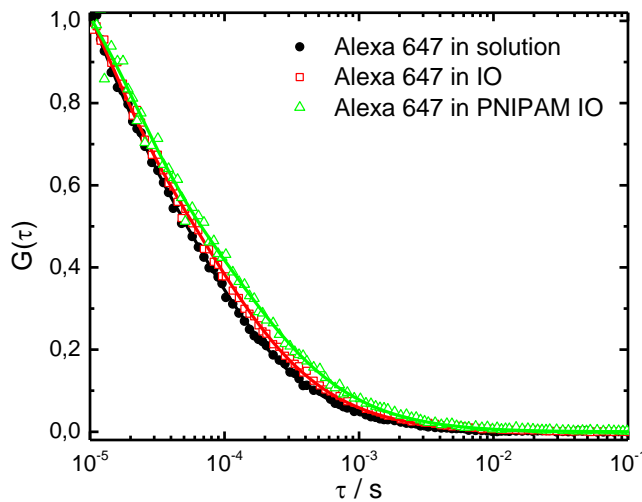


Figure 3.5. Normalized autocorrelation functions obtained for Alexa Fluor 647 diffusing in HPCE buffer solution (•), in silica iOpal filled with HPCE buffer solution (◻) and in PNIPAM modified silica inverse opal with HPCE buffer solution (△). The solid lines represent the corresponding fits.

In order to compare the diffusion rate with the molecular weight of PNIPAM chains, I control the polymerization time and get shorter PNIPAM chains and lower molecular weight. The M_n of the short chain is 3100 g/mol and polydispersity is 1.2 determined by GPC. Figure 3.6a is the elution volume for the PNIPAM chains and Figure 3.6b is its molecular weight distribution. Figure 3.7c shows the autocorrelation curves of Alexa 647 diffuse in iOpal, short chain grafted iOpal and long chain grafted iOpal, and the short chain is sandwiched between the iOpal and long chain grafted iOpal, showing that the length of PNIPAM can adjust the size of the hole and have an effect on the mobility of Alexa 647 inside.

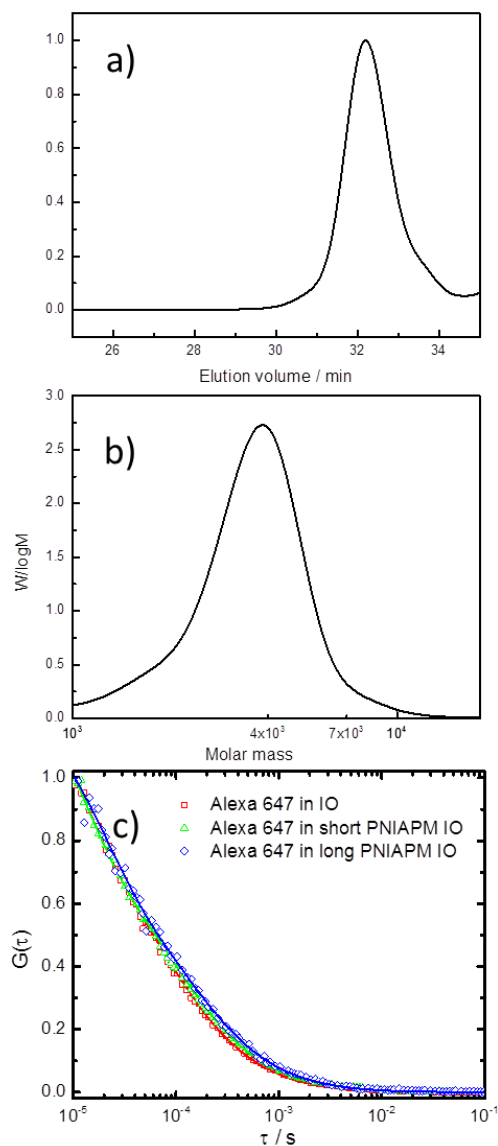


Figure 3.6. Gel-permeation chromatography results of the polymer with $M_n = 3100$ g/mol generated in the solution. (a) Elugram of the PNIPAM chains. (b) Molecular weight distribution. (c) Alexa 647 diffuses in bare iOpal and iOpal with different length of PNIPAM chains. Alexa Fluor 647 diffuse in silica iOpal filled with HPCE buffer solution (\square) and in short PNIPAM chains modified silica iOpal (Δ) and in long PNIAPM chains modified iOpal (\diamond). The solid lines represent the corresponding fits.

3.5 Tuning (controlling) the penetrant diffusion

Next I focus on the possibility to tune the diffusivity in the PNIPAM modified iOpal by controlling the temperature and thus the PNIPAM brush conformation and in turn the overall nanoporosity of the systems. In order to demonstrate this possibility the diffusion of Alexa 647 molecules was studied in buffer filled PNIPAM modified iOpal at various temperatures in the range 24 °C - 35 °C i.e. below and above the lower critical solution temperature of PNIPAM. For each measurement the system was kept at a constant temperature using a heating stage. The autocorrelation curves were recorded in the layer of the PNIPAM modified iOpal film (3 microns above the glass surface). Typical autocorrelation curves measured at temperatures of 24 °C and 35 °C are shown in Figure 3.7a. As fluorescence molecule will diffuse faster at higher temperature in aqueous solution[113, 114], Alexa 647 diffuse in iOpal without grafting PNIPAM is also shown as a comparison. In PNIPAM grafted iOpal, the curve measured at 35 °C is clearly shifted to short lag times indicating faster diffusion. Both curves can be well fitted with Equation 2.8 yielding diffusion times of 64 μ s and 122 μ s at 35 °C and 24 °C respectively, showing a diffusion speed up of 1.9 times. While this value is quite large, it should be kept in mind that even in free aqueous solution the temperature increase will speed up the diffusion. To estimate this effect we measured the diffusion time of Alexa 647 in the free solution above the iOpal and found a speed up of 1.4 times under the same temperature interval. The data clearly demonstrate a temperature induced speed-up of the penetrant mobility in PNIPAM modified silica inverse opal caused by the stretching and collapsing of polymer brushes inside the iOpal. Moreover, this change in mobility is fully reversible as confirmed by repeating the measurements after several heating and cooling cycles, as shown in Figure 3.7b- the diffusion time jumps between 64 μ s and 122 μ s as temperature changes.

There are two possible strategies to expand further the tunability range of penetrants' mobility in the PNIPAM modified iOpals: (i) to increase the length of the grafted brushes or (ii) to use larger penetrants. Here I explored the later possibility using

fluorescent penetrants quantum dots Qdot 525 with hydrodynamic radius of 5.6 nm. It's worth mentioning that the silica iOpal has strong interaction with QD 525 even though we use citrate buffer to avoid it [115]. Figure 3.7c shows the temperature dependence of the measured diffusion coefficient of QD 525 in the PNIPAM modified iOpal and same speed up control of tracers is observed. QD 525 yields diffusion times of 655 μs and 1540 μs at 35 $^{\circ}\text{C}$ and 24 $^{\circ}\text{C}$ respectively, with the speeding up of 2.4 times. Both curves can also be well fitted with Equation 2.8.

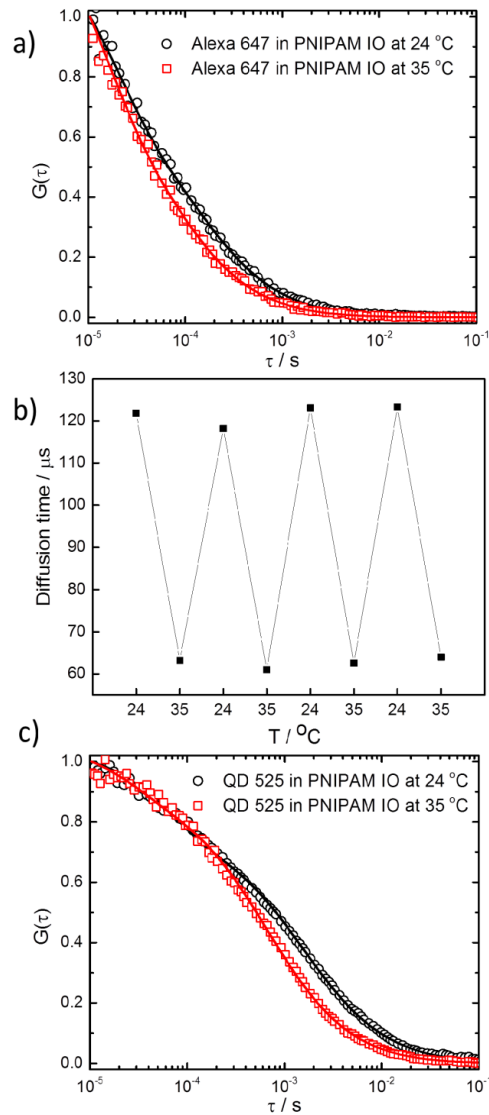


Figure 3.7. (a) Experimental autocorrelation curves for the diffusion of the Alexa 647 in PNIPAM grafted iOpal at 24 °C (circle) and 35 °C (square), respectively. (b) The diffusion time changes as temperature jumps of Alexa 647 in PNIPAM grafted iOpal. (c) Experimental autocorrelation curves for the diffusion of the QD 525 in PNIPAM grafted iOpal at 24 °C (circle) and 35 °C (square), respectively. The solid lines represent the corresponding fits with Equation 2.8.

Table 3.1 summarizes the diffusion time values measured for Alexa 647 and QD 525 in different environments and at different temperatures. These data demonstrate a temperature induced speed-up in the penetrants' mobility in PNIPAM modified silica iOpal caused by the stretching and collapsing of polymer brushes inside the iOpal.

Table 3.1. Diffusion time versus temperature of Alexa 647 and QD 525 in different environments and the speeding up percent accordingly.

	Diffusion time at 24 °C [μ s]	Diffusion time at 35 °C [μ s]	Speeding up factor
Alexa 647 in solution	56	40	1.4
Alexa 647 in PNIPAM iOpal	122	64	1.9
QD 525 in PNIPAM iOpal	1540	655	2.4

3.6 Conclusion

In this chapter I described the development of a new stimuli-responsive system, which combines two levels of nanoporosity. The system is based on silica iOpal, which

has well defined pore size and provide mechanical stability. After modifying the iOpal with temperature responsive polymer brushes, it becomes possible to change the size of the pores and thus control the mobility of small penetrants by simply tuning the temperature. This approach can be easily extended to other stimuli by using polymers that are responsive to e.g. pH or ionic strength.

CHAPTER 4

pH controlled diffusion of hairy nanoparticles

In this chapter, I consider control over the diffusion of pH-responsive hairy nanoparticles. To this end, fluorescent nanoparticles (hydrodynamic radius 20 nm) with polystyrene core and poly(*N*, *N*-diethylaminoethyl methacrylate) (PDEA) shell were prepared and used as a model system. Dynamic light scattering and turbidity measurements showed that the hydrophobic collapse of the hairs at high pH values is associated with strong inter-particle aggregation that hinders determination of individual particles size and mobility. However, at the ultra-low concentrations assessable by FCS (less than one particle per femto-litter) the aggregation was prevented. Thus, the pH induced change in the particles size and mobility, caused by the swelling or the collapse of the PDEA hairs was systematically measured and compared with that of individual freely diffusing PDEA chains under similar conditions. Finally, control over nanoparticle mobility in silica iOpal is also described.

4.1 Introduction and motivation

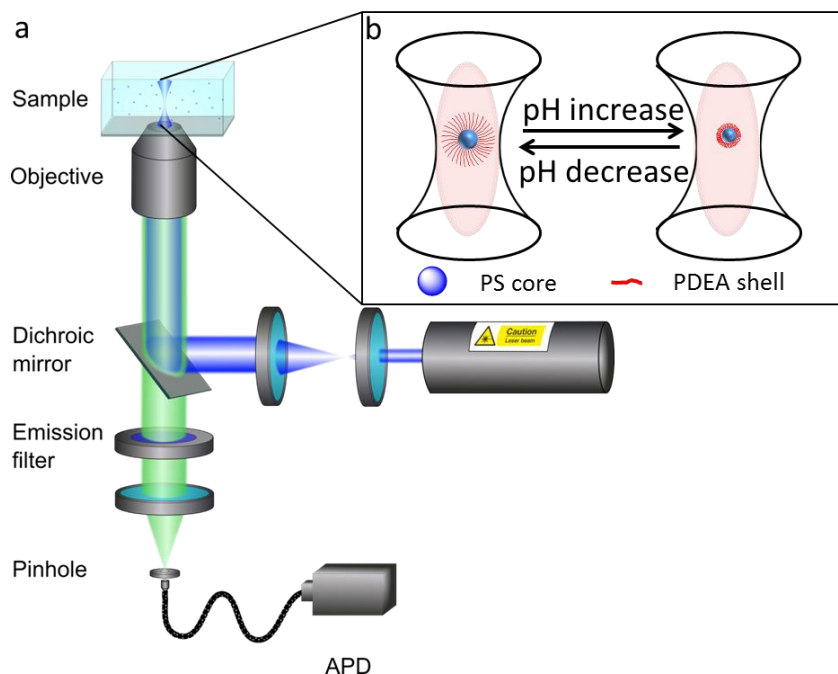
Stimuli-responsive polymer materials that can react to environmental changes[5, 116-118], e.g. of temperature, pH, light, electric fields, presence of ions, etc. are currently explored for their various applications[35-37, 119, 120] including drug delivery, smart biointerfaces, sensors, self-healing coatings, tunable catalysis, etc. Such materials can be used in different macromolecular configurations[5] including crosslinked polymer films, polymer brush layers, core-shell nanoparticles, capsules and nanogels. Among these configurations, hairy particles are used as drug carrier[121], catalyst supports[122], smart particulate emulsifiers[123], foam and liquid marble stabilizers[124], etc. In many of these applications the hairy particles are dispersed in

aqueous solutions and the response to environmental changes takes place in the form of a collapse of the polymer hairs as a result of a change in their behavior from hydrophilic to hydrophobic. The hydrophobic collapse is often associated with strong inter-particle aggregation.^[14] For example pH-responsive poly(*N*, *N*-diethylaminoethyl methacrylate) (PDEA) hairy particles are dispersed well in acidic aqueous media, but flocculated in basic aqueous media.[125] A controlled design of such systems and a precise control over the transition requires proper characterization of the hairy particles and good understanding of the hydrophobic collapse. To achieve these goals various characterization techniques such as X-ray photoelectron spectroscopy, transmission electron microscopy, atomic force microscope, scanning probe oxidation lithography, variable temperature ¹H NMR spectroscopy analysis, contact angle measurement, small-angle neutron scattering or dynamic light scattering have been used.[126-131] However, while these techniques can provide valuable information on the particle morphology and on the stimuli induced hydrophobic collapse in general, it is still a major experimental challenge to monitor and study the collapse on a single particle level, especially for very small nanoparticles. Thus, for many systems it is still unclear how exactly the conformation of the polymer “hairs” changes upon the application of the external stimuli and how these changes compare to systems where the same polymer is grafted as a brush on a solid surface or is a freely diffusing as an individual chain. In fact, even a measurement of the change of the individual hairy particle size upon the stimuli induced transition is often difficult or impossible, because the hydrophobic collapse is commonly associated with strong aggregation that prevents the evaluation of individual particle sizes with techniques such as DLS for example.

In this respect, fluorescence correlation spectroscopy (FCS) that is a powerful technique for studying the dynamics of fluorescent species such as small molecules, macromolecules, or nanoparticles in various environments offers an interesting alternative.[44] In FCS, the fluorescent intensity fluctuations caused by the diffusion of the species through a very small confocal detection volume are recorded and analyzed to obtain their diffusion coefficients, hydrodynamic radius, and concentrations. Due to its

high, single molecule sensitivity FCS can be used to measure the hydrodynamic radius of hairy nanoparticles in extremely dilute dispersions, in which the hydrophobic particle aggregation may be prevented. While initially developed and still predominantly used as a tool in molecular and cell biology, FCS has also found many applications in polymer and colloid science.[45, 46, 132] Furthermore, the method was previously applied to investigate stimuli-responsive polymer systems. For example the pH or salt concentration induced changes in the size of individual polymer chains[48, 49], or in the interaction between small molecules and grafted polyelectrolyte brushes[50, 51], as well as, the temperature responsiveness of Poly(*N*-isopropylacrylamide) (PNIPAM) microgel particles[52], and grafted hydrogel films[53, 54] were studied.

In this chapter I demonstrate how FCS can be used to directly monitor the hydrophobic collapse of pH-responsive hairy nanoparticle at individual particle level. To this end I prepared small fluorescent core-shell hairy nanoparticles with polystyrene core and PDEA shell and used them as a model system. PDEA is a pH-responsive polymer with biocompatibility and antibacterial activity that have been previously considered for applications such as gene delivery, pH-responsive controlled release, etc.[23-25] Using FCS I have systematically measured the pH dependent swelling and collapse on a single particle level and compared it to the behavior of individual freely diffusing PDEA chains under similar conditions, the scheme is shown in Scheme 4.1.



Scheme 4.1. (a) FCS setup[47] and (b) pH-responsive hairy nanoparticles.

4.2 Preparation of Bodipy labeled PS/PDEA hairy nanoparticle and PDEA single chain

... provided the Bodipy labeled PS/PDEA hairy nanoparticle and PDEA chains for me. The hairy nanoparticles are composed of crosslinked PS core and pH-responsive PEDA hairs. Bodipy is covalently connected onto the hairy PS. Detailed synthesis can be found in paper[75]. The scheme of the hairy nanoparticle is shown in scheme 4.1b. Number-average molecular weight (M_n) and molecular weight distribution (M_w/M_n) of PDEA hairs were estimated by gel-permeation chromatography (GPC) to be 1.55×10^4 g/mol and 1.14, respectively. The single PDEA chain with M_n and M_w/M_n were estimated by GPC to be 1.80×10^4 g/mol and 1.17, respectively.

The Bodipy was chosen as a fluorescent label because it is hydrophobic and according to the supplier information its fluorescence is relatively insensitive to solvent

polarity and pH changes. The fluorescent labeling was done by reacting the pendant primary amino groups in the shell with succinimidyl ester group-containing Bodipy dye. UV-vis absorption and fluorescence spectra for PDEA-P(S/Bodipy) in water were measured to confirm the introduction of Bodipy (Figure 4.2). While the results clearly show that the dye is attached to the nanoparticles, they also indicate a strong decrease of fluorescence with the increase of pH. The concentration under pH 4, 7.5 and 12 was kept at 0.14 g/L. Similar effect was observed in the FCS studies (see Table 4.1). On the other hand, the spectra on Figure 4.2a show that the dye absorption properties are almost independent on the pH. The number of Bodipy dyes per nanoparticle was estimated by dividing the molar extinction coefficient of PDEA-P(S/Bodipy) nanoparticles to that of Bodipy molecules. This yielded a value of ≈ 9 that is consistent with estimates based on FCS measurements of the fluorescent brightness of the nanoparticles and the individual dye molecules.

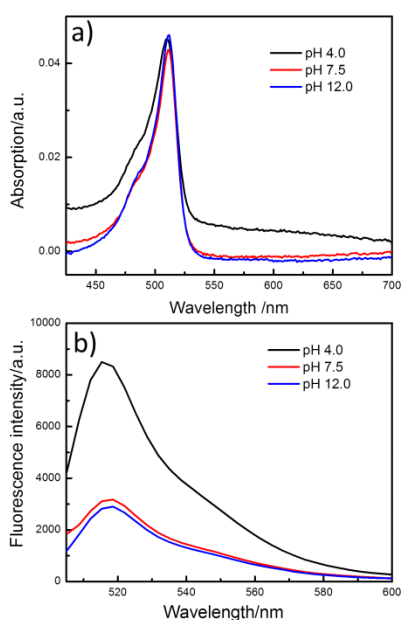


Figure 4.2. Absorption and fluorescence spectra of Bodipy labeled PS/PDEA hairy nanoparticles.

Table 4.1. Fluorescence brightness of the hairy nanoparticles as measured by FCS at different pH.

pH	5.5	6.0	7.0	8.5	11.0	12.0
Fluor. brightness KHz/ particle	42.5	23.6	16.0	15.7	16.6	15.9

4.3 Monitoring the pH-responsive behavior at high concentration

I first investigated the pH-responsive behavior of the cross-linked PDEA-P(S/AEM) in aqueous dispersions with relatively high concentrations in the range 1 – 10 g/L using classical techniques like optical transmission measurements and dynamic light scattering (DLS). Figure 4.3 shows the pH dependence of the transmittance (%T) of an aqueous dispersion with concentration of 10 g/L measured at the wavelength of 600 nm. The pH value was varied by adding HCl or NaOH to the dispersion. Below pH 7, the %T value was virtually constant and close to 100 %. In this pH range the pendent tertiary amine groups in PDEA shells are protonated, the polymer hairs are hydrophilic and thus the small nanoparticles are well dispersed in the aqueous environment. However %T decreased sharply as the pH increased above 7. This increase in turbidity is caused by inter-particle aggregation occurring at higher pH due to hydrophobic interactions between the pendant deprotonated amine groups in PDEA shells.

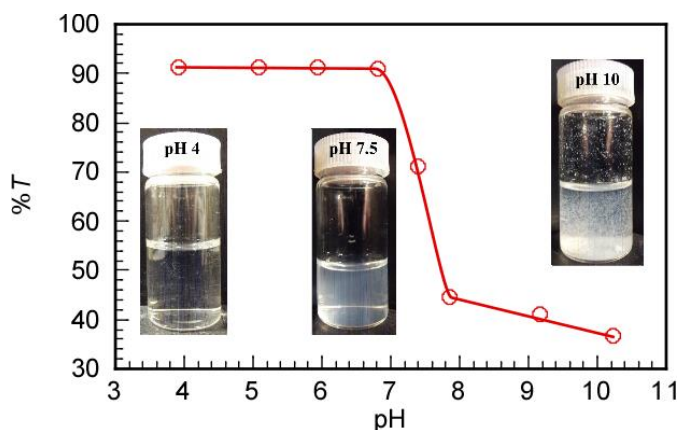


Figure 4.3. Transmittance (% T) at 600 nm for aqueous dispersions of PDEA-P(S/AEM) particles as a function of pH at $C_p = 10$ g/L. Inserts are photographs of aqueous dispersions of PDEA-P(S/AEM) particles at pH 4, 7.5, and 10. (Provided by ...)

Next, aqueous dispersion of the PDEA-P(S/AEM) nanoparticles with concentration of 1 g/L, i.e. ten times lower than that used for the turbidity measurements were characterized by dynamic light scattering (DLS). To remove impurities and occasional large aggregates the dispersions were filtrated through 0.2- μm filters prior to the DLS measurements. Typical results in the form of hydrodynamic radius (R_h) distributions are shown in Figure 4.4a. The corresponding average R_h values at pH 4 and 10 were 25.4 nm and 71.2 nm, respectively. To investigate the pH-responsive behavior of PDEA-P(S/AEM) in water, the pH dependence of R_h was measured (Figure 4.4b). Below pH 7, the R_h value was virtually constant at about 25 nm. However, R_h increased sharply as the pH increased from 7 to 8, reaching a new plateau value of around 70 nm.

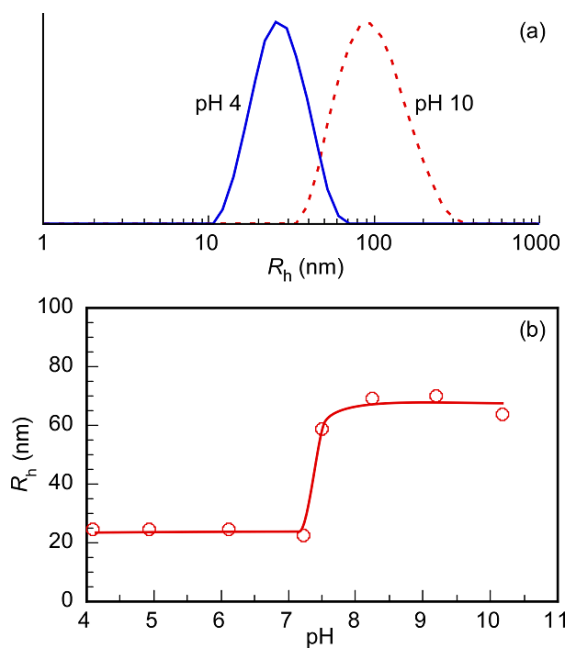


Figure 4.4. (a) DLS data for the distribution of the hydrodynamic radius (R_h) of PDEA-P(S/AEM) particles in aqueous dispersions with pH 4 (—) and pH 10 (---) at $C_p = 1$ g/L. (b) Average R_h of the particles as a function of pH. (Provided by ...)

These results indicated that even at the relatively low particle concentration of 1 g/L used in the DLS experiments the PDEA-P(S/AEM) nanoparticles still aggregate at high pH values due to hydrophobic interactions. This is further evident from the TEM images (Figure 4.5) of dried nanoparticle dispersions with different pH values. While at pH 4 individual particles are observed (Figure 4.5a) at pH 10 the particles tended to aggregate together. From the TEM images we could estimate that the average radius of the cross-linked PDEA-P(S/AEM) particles was 9.4 nm at pH 4.0. As can be expected, this value is significantly smaller than that of the hydrodynamic radius ($R_h \approx 25$ nm) estimated by DLS, due to the shrinking of the particles during drying and hydrodynamic effects. In spite of the aggregated morphology, the TEM image obtained for the dispersion with pH 10 (Figure 4.5b) reveals a decrease in the individual nanoparticle size compared to that at pH 4 (Figure 4.5a) and thus confirms the hydrophobic collapse of the PDEA hairs at high pH.

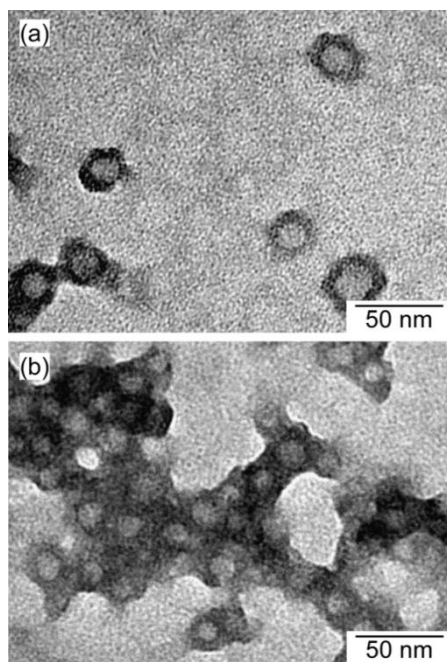


Figure 4.5. TEM images of PDEA-P(S/AEM) particles after drying from aqueous dispersions with (a) pH 4 and (b) pH 10. (Provided by Dr. ...)

4.4 Monitoring the pH-responsive behavior at individual particle level

In order to monitor pH dependent hydrophilic-hydrophobic transition of the PDEA hairs of individually dispersed nanoparticles we performed FCS experiments with highly diluted dispersions of Bodipy labeled nanoparticles. Again, the pH value was tuned by adding HCl and NaOH to the dispersions. The concentration of PDEA-P(S/Bodipy) under different pH conditions was always kept at 0.02 g/L, which is 50 times less than the concentration used in the DLS experiments. Typical FCS auto-correlation curves measured at various pH values are shown in Figure 4.6a. With increasing pH the curves shift to the shorter lag times, reflecting the decrease in particle size and thus the faster diffusion. The experimental auto-correlation curves could be well fitted with Equation 2.8 yielding the diffusion coefficients, and through the Stokes-Einstein relation, the hydrodynamic radius, R_h of the hairy nanoparticles. Figure 4.6b shows the R_h values obtained over broad pH range. The value at low pH, $R_h=23$ nm is very similar to that measured by DLS (Figure 4.4b), which confirms the accuracy of the FCS data. However, in contrast to the DLS studies, with the increase of pH, the measured hydrodynamic radius decreases continuously down to a value $R_h = 10$ nm at pH 12. These results show that at the very low concentrations assessable by FCS the particle aggregation caused by hydrophobic interactions can be strongly diminished and the pH-responsiveness of the PDEA hairs can be monitored on individual nanoparticle level. Moreover, compared to the DLS result (Figure 4.4b) the FCS data shown in Figure 4.6b reveal a less sharp transition that extends over a broad pH range. This effect may be related to the much lower concentration at which the FCS measurements were performed and possibly to the coexistence of PDEA hairs at different stage of the collapse at a given overall pH value.

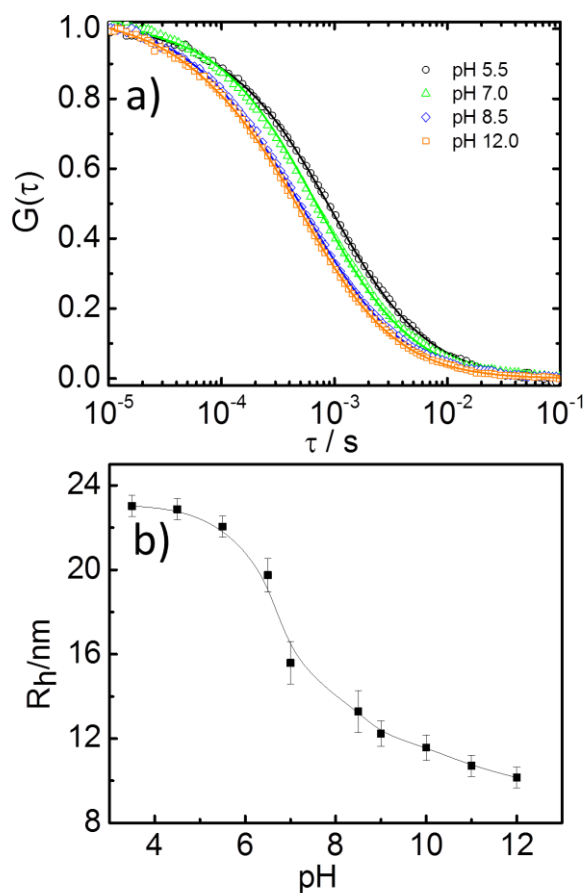


Figure 4.6. (a) Normalized, experimental FCS autocorrelation curves measured for aqueous dispersions of Bodipy labeled nanoparticles at $C_p = 0.02$ g/L and different pH values. The solid lines represent the corresponding fits with Equation 2.8. (b) Hydrodynamic radius R_h of the nanoparticles as a function of pH. The solid line is to guide the eye.

The results summarized in Table 4.2 clearly demonstrate that depending on the experimental conditions different techniques may provide different values for the nanoparticle size and this may lead to certain confusion if the experimental conditions are not well specified. For the system considered here at low pH values (pH 4) the PDEA shell of the nanoparticles is hydrophilic and they are well dispersed (not aggregating) over broad concentration range. At these conditions both DLS and FCS

provide very similar values for the hydrodynamic radius, i.e. 25.4 ± 3 nm and 22.8 ± 3 nm respectively. At high pH values (pH 10) the PDEA shell of the nanoparticles exhibits hydrophobic collapse and the hydrodynamic radius of the individual nanoparticles decreases to around 12 ± 2 nm as measured by FCS at very low concentrations of 0.02 g/L. DLS could not track this effect because at the higher concentration needed for DLS (1 g/L) the hydrophobic collapse is associated with particles aggregation and thus DLS measures an average aggregate hydrodynamic radius of around 70 nm. On the other hand for the TEM studies nanoparticles have to be studied in the dry state that leads to complete shrinking of the nanoparticles and systematically lower values for their size. It is important to emphasize at this point that depending on the experimental conditions different techniques may provide different values for the nanoparticles size (Table 4.2), and therefore the exact experimental conditions should be always carefully considered.

Table 4.2. R_h of hairy nanoparticles measured by DLS, FCS and TEM.

	DLS	FCS	TEM
Concentration (g/L)	1.0	0.02	dry
Particle size at pH 4 (nm)	25.4	22.8	9.4
Particle size at pH 7.5 (nm)	40.0	15.0	-
Particle size at pH 10 (nm)	71.2	11.8	aggregation

Such experimental condition is example the concentration that is different for the DLS and FCS studies (Table 4.2). In order to further illustrate this, I used dispersion of hairy nanoparticle with 1.0 g/L concentration, the same concentration of DLS

measurement and studied it by FCS. Figure 4.7 shows the autocorrelation curves of hairy nanoparticle in aqueous solution of pH = 5.0 and pH = 7.5. It clearly shows that at pH = 7.5, the curve shift to long lag times indicating slower diffusion and bigger size, which is in accordance with the DLS result, confirming that the concentration plays a big rule on the dispersed state of hairy nanoparticles.

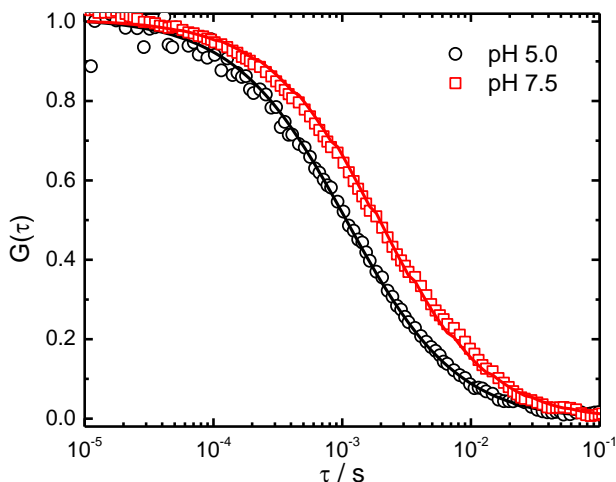


Figure 4.7. Autocorrelation functions $G(\tau)$ for the diffusion of the hairy nanoparticle at 1 g/L. (The same concentration of DLS measurement)

Next, I studied the reversibility of the pH induced collapse on the grafted PDEA chains. Therefore, we consecutively tuned the pH of the nanoparticle dispersion between 4.0 and 11. Figure 4.8a are the autocorrelation curves of hairy nanoparticles at pH = 4.0 and pH = 11.0. As shown in Figure 4.8b, the hydrodynamic radius of the particles changed reversibly from 23 nm at low pH to 11 nm at high pH values. The cycle was repeated only 3 times because the continuous addition of NaOH and HCl solutions to the dispersion increased its total volume and thus decreased the concentration of the nanoparticles to the edge of the FCS sensitivity.

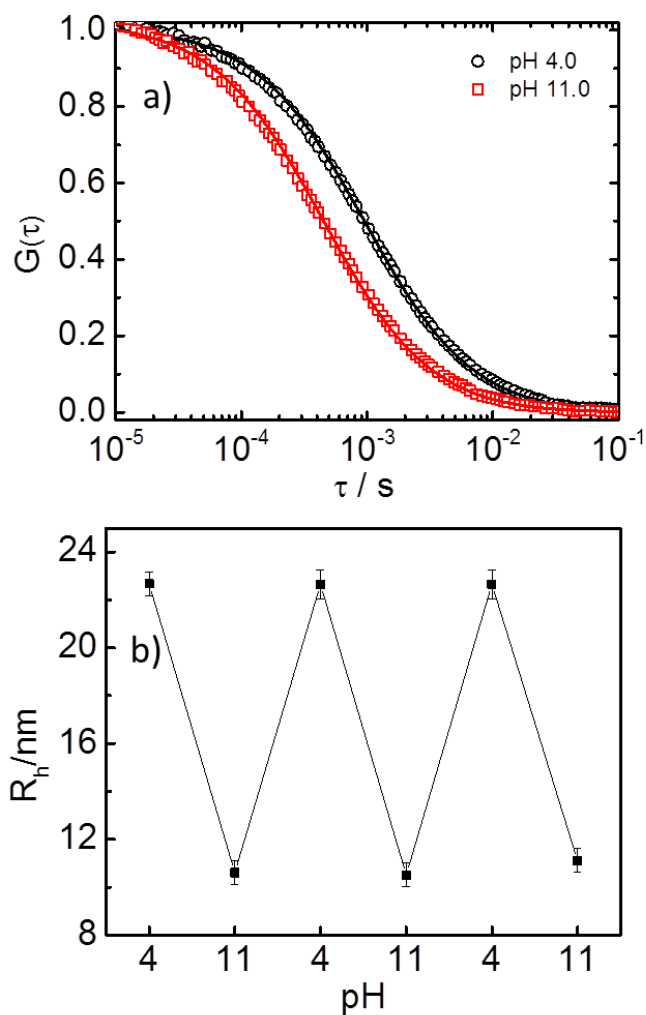


Figure 4.8. (a) Autocorrelation curve of hairy nanoparticles at pH = 4.0 and pH = 11.0. The solid lines represent the corresponding fits with Equation 2.8. (b) Hydrodynamic radius, R_h , as a function of pH upon cycling the pH value between 4.0 and 11.0.

4.5 Comparison of the pH-responsiveness of the hairy nanoparticles and single chains

In an attempt to compare the pH induced collapse of PDEA chains attached to the surface of a nanoparticle and to that of freely diffusing chains, Bodipy-labeled

polymer (P(DEA/Bodipy)) was prepared as described in the experimental part and the hydrodynamic radius of the individual chains was measured with FCS. The experiments were performed in extremely diluted solutions (0.003 g/L) at various pH. Under acid conditions, the polymer chains were well dispersed in the solution. FCS autocorrelation curves (Figure 4.9a) could easily be recorded and the individual chain hydrodynamic radius could be calculated (Figure 4.9b). As expected, the hydrodynamic radius continuously decreased with the increase of pH, reflecting the hydrophobic collapse of the chains. However, as discussed above the increase of pH leads to a strong decrease in the fluorescent brightness of the Bodipy labels. Furthermore, the PDEA chains carry only one dye per chain and thus their fluorescent brightness is significantly weaker than that of the nanoparticles (with ~9 dyes per particle). Due to these reasons and possibly some additional hydrophobic effects, e.g. chain migration to the water/air interface of the sample chamber, we were not able to record reasonable FCS autocorrelation curves and determine the hydrodynamic radius of individual PDEA chains at high pH values. The data shown in Figure 4.9 indicates that when the pH increased from 2.3 to 5.1 the hydrodynamic radius of the P(DEA/Bodipy) chains ($M_n = 18000$ g/mol) decreased from 2.9 nm to 2.2 nm, i.e. with 0.7 nm (hydrodynamic diameter decreased with 1.4 nm). For comparison the hydrodynamic radius of the nanoparticles processing grafted PDEA hairs with similar molecular weight ($M_n = 15500$ g/mol) decreased by 1.6 nm in the same pH range (Figure 4.9b). While the estimated hydrodynamic radius (diameters) should be considered only as an approximation for the real chain dimensions, the obtained values indicate that the chains grafted to the PS nanoparticles contract in a similar way and to similar extend compared to freely diffusing chains.

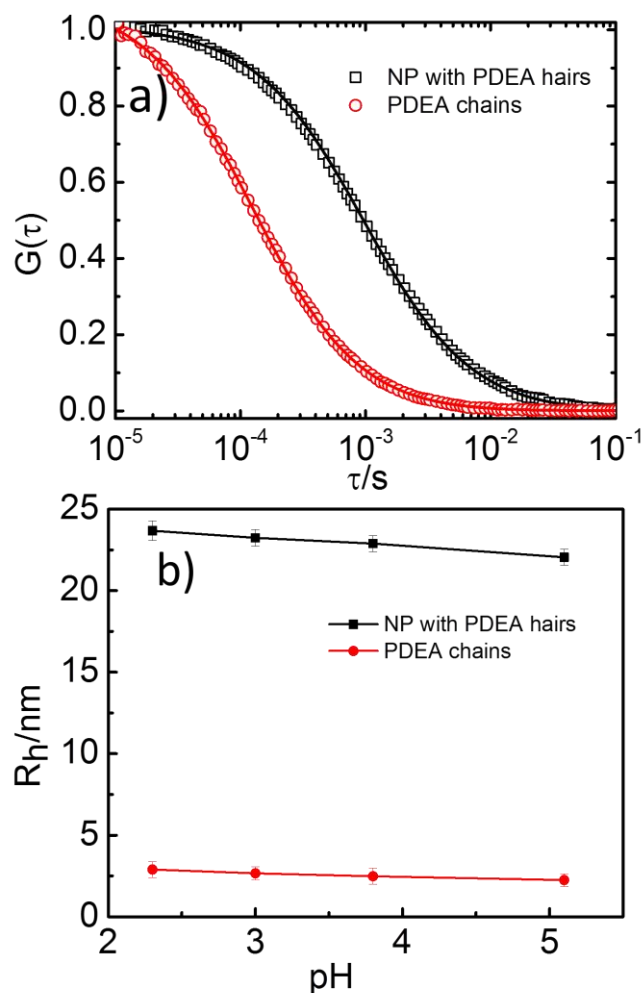


Figure 4.9. (a) Autocorrelation curves of PDEA hair and PDEA single chain at pH 3.0. The solid lines represent the corresponding fits with Equation 2.8. (b) Plot of R_h as a function of pH for PDEA hairs (0.02 g/L).and single chain solution (0.003 g/L).

4.6 Controlling the mobility of the pH-responsive particles in nanoporous environment

Some of the most important applications of the stimuli-responsive nanoparticles are related to the possibility to control their mobility in nanoporous media. In such

environment even small changes of the particle size may have a profound effect on the mobility. With this in mind, we studied the diffusion of the PDEA-P(S/Bodipy) nanoparticles (PDEA-P(S/Bodipy)) in a water filled silica inverse opal at various pH values.

A silica inverse opal consists of a regular arrangement of spherical voids surrounded by solid silica walls with interconnecting circular pores. It was chosen as a model for well-defined nanoporous structure.[73, 74, 86, 87] The particular structure used in this study (Figure 2.9c in chapter 2) had a void diameter of 920 nm and interconnecting pores diameter of 240 nm. It was infiltrated with aqueous dispersion of the PDEA-P(S/Bodipy) nanoparticles. The particles' diffusion coefficient was measured with FCS. Prior to the FCS measurements the structure was imaged using the reflection mode of the confocal microscope in order to confirm the regular porosity and the absence of defects (Figure 4.10a) at the point where the FCS measurements were performed. Figure 4.10b shows typical FCS autocorrelation curves measured in the inverse opal at pH = 9.0 and pH = 4.0. For comparison the autocorrelation curves measured in free aqueous environment (without inverse opal) are also shown. It should be noted that because the nanoparticle's diffusion is confined in the inverse opal voids, which have sizes similar to that of the FCS probing volume, the use of Equation 2.8 that is derived for free 3D diffusion is not trivial. However, as Equation 2.8 represents very well the experimentally measured autocorrelation curves (Figure 4.10b) we still used it as a preliminary, approximate way to estimate the diffusion coefficients of the nanoparticles in the inverse opals. The curves measured in the inverse opal are shifted to the longer lag times, reflecting the significantly slower diffusion in the nanoporous structure. Furthermore, the change in pH from 4.0 to 9.0 affects significantly stronger the mobility of the nanoparticles in the inverse opal. To quantify this effect we have fitted the autocorrelation curves with Equation 2.8 and determined the respective diffusion coefficients of the nanoparticles. In free aqueous environment the diffusion coefficient increased from $1.0 \times 10^{-11} \text{ m}^2/\text{s}$ to $2.0 \times 10^{-11} \text{ m}^2/\text{s}$ when the pH was changed from 4.0 to 9.0. The corresponding values in silica inverse opal were from 4.0×10^{-12}

m^2/s to $1.05 \times 10^{-11} \text{ m}^2/\text{s}$, respectively. Thus, the pH induced change in mobility (diffusion coefficient) was significantly larger in the silica inverse opal, reflecting the stronger effect of the nanoparticle size on the mobility in the porous environment.

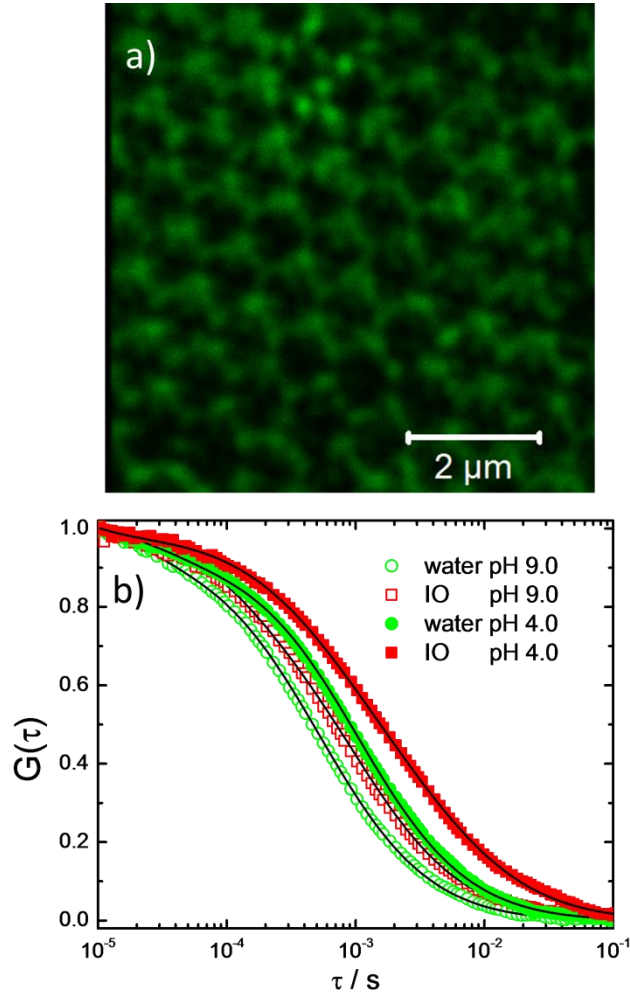


Figure 4.10. (a) A confocal microscopy image (in reflection mode) of water infiltrated silica inverse opal. (b) Experimental autocorrelation curves for the diffusion of the Bodipy labeled hairy nanoparticle in the iOpal made from 1 μm PS particles (red squares) and in free aqueous environment (green circles) at pH 9.0 (open symbols) and pH 4.0 (solid symbols). The solid lines represent the corresponding fits with Equation 2.8.

Another inverse opal made from 330 nm PS nanoparticles is also used as a model for well-defined nanoporous structure (SEM image is shown in Figure 2.9b in chapter 2 and reflectance mode image by FCS is shown in Figure 3.1 in chapter 3). Figure 4.11 also shows the change in pH from 4.0 to 9.0 affects significantly stronger the mobility of the nanoparticles in the inverse opal. The autocorrelation curves were fitted with Equation 2.8 and determined the respective diffusion coefficients of the nanoparticles. In the smaller hole with 315 nm in diameter, the diffusion coefficient in silica iOpal was from $3.0 \times 10^{-12} \text{ m}^2/\text{s}$ to $7.2 \times 10^{-12} \text{ m}^2/\text{s}$ from 4.0 to 9.0, respectively. These values show that in smaller iOpal the mobility control of the tracer is more significant than free aqueous solution.

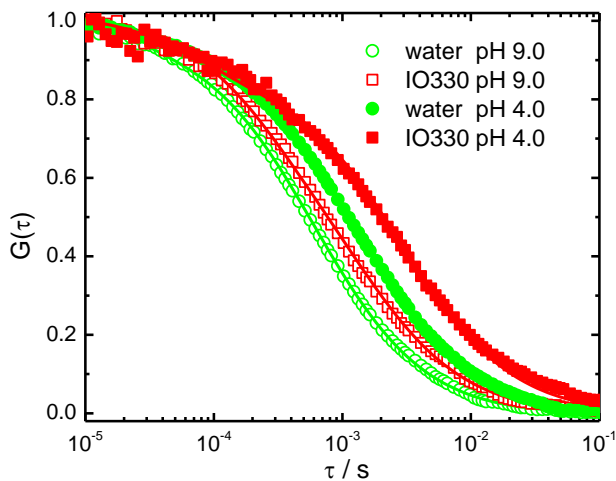


Figure 4.11. Experimental autocorrelation curves for the diffusion of the Bodipy labeled hairy nanoparticle in the iOpal made from 330 nm nanoparticle (red squares) and in free aqueous environment (green circles) at pH 9.0 (open symbols) and pH 4.0 (solid symbols). The solid lines represent the corresponding fits with Equation 2.8.

4.7 Conclusion

I showed that due to its very high sensitivity FCS can be used to measure the stimuli-responsiveness of individual hairy nanoparticles. Using this technique I found that when the pH is increased, PDEA chains grafted to a small polystyrene core collapse similarly to freely diffusing PDEA chains. The particle concentration plays an important role on the general behavior of stimuli-responsive hairy nanoparticles. At high and moderately low concentrations, the pH induced collapse leads to aggregation and thus lowering of the nanoparticles mobility. At very low concentrations, however, the hydrophobic collapse is associated with decrease of nanoparticles size and increase in their mobility. The later effect is particularly evident and important when the nanoparticles are dispersed in nanoporous environment.

CHAPTER 5

Summary and conclusion

Controlling the mobility of molecules, macromolecules, nanoparticles etc. in solution and in complex, nanostructured environments is of vital importance, as diffusion is the dominant mechanism for the transport of such species in e.g. solid nanoporous structures, polymer solutions and gels, or in living cells. In this thesis I described how using stimuli-responsive polymers, one can design a stimuli-responsive system in which the mobility of molecules and nanoparticles in solution or nanoporous environment can be controlled, and the whole process can be monitored *in situ* by fluorescence correlation spectroscopy (FCS).

First, I prepared silica inverse opals (iOpal), which are well-defined, highly ordered porous structures and with high mechanic stability. By modifying iOpal with poly(N-isopropylacrylamide) (PNIPAM) I obtained a stimuli-responsive system with two levels of porosity. By simply tuning the temperature below or above the lower critical solution temperature of PNIPAM, it was possible to change the size of the pores and thus control the mobility of small species in them. Moreover, the mobility changes caused by the PNIPAM brushes as temperature changes were fully reversible after several heating and cooling cycles. In this way the mobility of the small species is controllable by just immersing them in the responsive nanoporous environment.

Second, I prepared the PS/PDEA hairy nanoparticles with pH-responsive hairs. Owing to the high, single molecule sensitivity of FCS, colloid aggregation of hairy nanoparticles can be avoided and the pH induced collapse of hairs can be monitored at very low concentration, which means I can observe the hydrophobic collapse of pH-responsive hairy nanoparticles at individual particle level. By increasing the pH of the solution gradually, the hairs would collapse accordingly, thus the size of hairy nanoparticle would decrease and they would show faster mobility. Furthermore, I found

that PDEA chains grafted to a small polystyrene core collapse similarly to freely diffusing PDEA chains as pH in solution changes. When the nanoparticles are dispersed in nanoporous environment, faster mobility induced by decreased nanoparticle size is particularly evident. In this way I prepared responsive nanoparticles which show controllable mobility in diverse environments.

In brief, I have produced stimuli-responsive systems, in which one can control the mobility control of species in aqueous solutions and confined nanoporous environments. Owing to the high sensitivity of FCS technique, this effect can be monitored *in situ* and the mobility of the species can be traced.

Acknowledgement

...

List of symbols

C	Concentration in dimensions
D or D_i	Diffusion coefficient of species i
F	Force
$F(t')$	Fluorescence intensity (kHz) at time t'
f_i	Fraction of species i
$G(\tau)$	Autocorrelation function
G	Gibbs free energy
λ	Wavelength of light
λ_{ex}	Wavelength of excitation light
λ_{em}	Wavelength of emission light
J	Diffusion flux
k_B	Boltzmann constant
M_n	Number average molecular weight
M_w	Weight average molecular weight
n	Refractive index
N	Number of monomers in polymer chain
N_A	Avogadro's number

Np	number of particles in the observation volume
$\langle \Delta r^2(t) \rangle$	Mean square displacement
R_h	Hydrodynamic radius
r_0	Radial axis of confocal volume
S	Structure of parameter ($= z_0/r_0$)
t	Experimental lag time
τ_D	Lateral diffusion time
T	Temperature
T_0	Ideal glass transition temperature
T_g	Glass transition temperature
V	Observation volume
v	Particle moving speed
z_0	Vertical axis of confocal volume
η	Viscosity
∇	Gradient operator
Δ	Laplacian, the second derivative
μ	Particle mobility
r	Radius of particle
q	Electrical charge
ϕ	Weight fraction

List of abbreviations

ATRP	Atom transfer radical polymerization
DLS	dynamic light scattering
FCS	Fluorescence correlation spectroscopy
GPC	Gel Permeation Chromatography
NA	Numerical aperture
NMR	Nuclear magnetic resonance
PDEAEMA	Poly(2-diethylaminoethyl methacrylate)
PNIPAM	Poly (N-isopropylacrylamide)
PS	Polystyrene
Qdot	Quantum dot
VD	Vertical deposition
THF	Tetrahydrofuran

References

1. Einstein, A., *Über die von der molekularkinetischen Theorie der Wärme geforderte Bewegung von in ruhenden Flüssigkeiten suspendierten Teilchen*. Ann. Phys. , 1905. **17**: p. 549–560.
2. Fick, A., *Ueber Diffusion*. Ann. der. Physik, 1855. **94**: p. 59-86.
3. Fick, A., *On liquid diffusion*. Journal of Membrane Science, 1995. **100**: p. 33-38.
4. Smoluchowski, M., *Zur kinetischen Theorie der Brownschen Molekularbewegung und der Suspensionen*. Ann. der. Physik, 1906. **326**(14): p. 756-780.
5. Stuart, M.A.C., et al., *Emerging applications of stimuli-responsive polymer materials*. Nature Materials, 2010. **9**(2): p. 101-113.
6. Grubbs, R.B. and Z. Sun, *Shape-changing polymer assemblies*. Chemical Society Reviews, 2013. **42**(17): p. 7436-7445.
7. Roy, D., W.L.A. Brooks, and B.S. Sumerlin, *New directions in thermoresponsive polymers*. Chemical Society Reviews, 2013. **42**(17): p. 7214-7243.
8. Scarpa, J.S., D.D. Mueller, and I.M. Klotz, *Slow hydrogen-deuterium exchange in a non-.alpha.-helical polyamide*. Journal of the American Chemical Society, 1967. **89**(24): p. 6024-&.
9. Zhai, L., *Stimuli-responsive polymer films*. Chemical Society Reviews, 2013. **42**(17): p. 7148-7160.
10. Ward, M.A. and T.K. Georgiou, *Thermoresponsive Polymers for Biomedical Applications*. Polymers, 2011. **3**(3): p. 1215-1242.
11. Peng, T. and Y.L. Cheng, *Temperature-responsive permeability of porous PNIPAAm-g-PE membranes*. Journal of Applied Polymer Science, 1998. **70**(11): p. 2133-2142.
12. Chang, Y., et al., *Tunable Bioadhesive Copolymer Hydrogels of Thermoresponsive Poly(N-isopropyl acrylamide) Containing Zwitterionic Polysulfobetaine*. Biomacromolecules, 2010. **11**(4): p. 1101-1110.
13. Haraguchi, K., K. Uyama, and H. Tanimoto, *Self-healing in Nanocomposite Hydrogels*. Macromolecular Rapid Communications, 2011. **32**(16): p. 1253-1258.
14. Gibson, M.I. and R.K. O'Reilly, *To aggregate, or not to aggregate? considerations in the design and application of polymeric thermally-responsive nanoparticles*. Chemical Society Reviews, 2013. **42**(17): p. 7204-7213.
15. M. Heskins, J.E.G., *Solution Properties of Poly(Nisopropylacrylamide)*. J. Macromol. Sci.- Chem, 1968. **2**(8): p. 1441-1455.
16. Chen, G.H. and A.S. Hoffman, *Graft copolymers that exhibit temperature-induced phase transitions over a wide range of pH*. Nature, 1995. **373**(6509): p. 49-52.
17. Kujawa, P., et al., *Impact of end-group association and main-chain hydration on the thermosensitive properties of hydrophobically modified telechelic poly(N-isopropylacrylamides) in water*. Macromolecules, 2006. **39**(1): p. 341-348.

18. Schmaljohann, D., *Thermo- and pH-responsive polymers in drug delivery*. *Advanced Drug Delivery Reviews*, 2006. **58**(15): p. 1655-1670.
19. Kharlampieva, E., et al., *Hydrogen-bonded multilayers of thermoresponsive polymers*. *Macromolecules*, 2005. **38**(25): p. 10523-10531.
20. Chunder, A., et al., *Conformal switchable superhydrophobic/hydrophilic surfaces for microscale flow control*. *Colloids and Surfaces a-Physicochemical and Engineering Aspects*, 2009. **333**(1-3): p. 187-193.
21. Huber, D.L., et al., *Programmed adsorption and release of proteins in a microfluidic device*. *Science*, 2003. **301**(5631): p. 352-354.
22. Zhou, Y.M., et al., *Deposition transfection technology using a DNA complex with a thermoresponsive cationic star polymer*. *Journal of Controlled Release*, 2007. **123**(3): p. 239-246.
23. Dai, S., P. Ravi, and K.C. Tam, *pH-Responsive polymers: synthesis, properties and applications*. *Soft Matter*, 2008. **4**(3): p. 435-449.
24. Tang, Y.Q., et al., *Solubilization and controlled release of a hydrophobic drug using novel micelle-forming ABC triblock copolymers*. *Biomacromolecules*, 2003. **4**(6): p. 1636-1645.
25. Tian, W., et al., *Multiresponsive Properties of Triple-Shell Architectures with Poly(N,N-diethylaminoethyl methacrylate), Poly(N-vinylcaprolactam), and Poly(N,N-dimethylaminoethyl methacrylate) as Building Blocks*. *Macromolecular Chemistry and Physics*, 2012. **213**(23): p. 2450-2463.
26. Alexander, S., *Adsorption of chain molecules with a polar head a scaling description*. *Journal De Physique*, 1977. **38**(8): p. 983-987.
27. Degennes, P.G., *Conformations of polymers attached to an interface*. *Macromolecules*, 1980. **13**(5): p. 1069-1075.
28. Milner, S.T., *Polymer Brushes*. *Science*, 1991. **251**(4996): p. 905-914.
29. Zhou, C., M.A. Hillmyer, and T.P. Lodge, *Micellization and Micellar Aggregation of Poly(ethylene-alt-propylene)-b-poly(ethylene oxide)-b-poly(N-isopropylacrylamide) Triblock Terpolymers in Water*. *Macromolecules*, 2011. **44**(6): p. 1635-1641.
30. Ishida, N. and S. Biggs, *Salt-induced structural behavior for poly(N-isopropylacrylamide) grafted onto solid surface observed directly by AFM and QCM-D*. *Macromolecules*, 2007. **40**(25): p. 9045-9052.
31. Laloyaux, X., et al., *Surface and Bulk Collapse Transitions of Thermo responsive Polymer Brushes*. *Langmuir*, 2010. **26**(2): p. 838-847.
32. Bradley, C., et al., *Response Characteristics of Thermoresponsive Polymers Using Nanomechanical Cantilever Sensors*. *Macromolecular Chemistry and Physics*, 2009. **210**(16): p. 1339-1345.
33. Hoffman, A.S., *The origins and evolution of "controlled" drug delivery systems*. *Journal of Controlled Release*, 2008. **132**(3): p. 153-163.
34. Hayashi, G., et al., *Photoregulation of a peptide-RNA interaction on a gold surface*. *Journal of the American Chemical Society*, 2007. **129**(28): p. 8678-8679.

35. Tokareva, I., et al., *Nanosensors based on responsive polymer brushes and gold nanoparticle enhanced transmission surface plasmon resonance spectroscopy*. Journal of the American Chemical Society, 2004. **126**(49): p. 15950-15951.
36. Urban, M.W., *Intelligent polymeric coatings; Current and future advances*. Polymer Reviews, 2006. **46**(4): p. 329-339.
37. Lu, Y., et al., *Thermosensitive core-shell particles as carriers for Ag nanoparticles: Modulating the catalytic activity by a phase transition in networks*. Angewandte Chemie-International Edition, 2006. **45**(5): p. 813-816.
38. Oishi, M., et al., *Endosomal release and intracellular delivery of anticancer drugs using pH-sensitive PEGylated nanogels*. Journal of Materials Chemistry, 2007. **17**(35): p. 3720-3725.
39. Hervet, H., L. Leger, and F. Rondelez, *Self-Diffusion in Polymer Solutions: A Test for Scaling and Reptation*. Physical Review Letters, 1979. **42**(25): p. 1681-1684.
40. Vaz, W.L.C., et al., *Size dependence of the translational diffusion of large integral membrane proteins in liquid-crystalline phase lipid bilayers. A study using fluorescence recovery after photobleaching*. Biochemistry, 1982. **21**(22): p. 5608-5612.
41. Callaghan, P.T. and D.N. Pinder, *A pulsed field gradient NMR study of self-diffusion in a polydisperse polymer system: dextran in water*. Macromolecules, 1983. **16**(6): p. 968-973.
42. Schillen, K., W. Brown, and R.M. Johnsen, *Micellar Sphere-to-Rod Transition in an Aqueous Triblock Copolymer System. A Dynamic Light Scattering Study of Translational and Rotational Diffusion*. Macromolecules, 1994. **27**(17): p. 4825-4832.
43. Jobic, H. and D.N. Theodorou, *Quasi-elastic neutron scattering and molecular dynamics simulation as complementary techniques for studying diffusion in zeolites*. Microporous and Mesoporous Materials, 2007. **102**(1-3): p. 21-50.
44. Rigler, R., E.S. Elson, *Fluorescence correlation spectroscopy: Theory and Applications*. Springer, 2001.
45. Papadakis, C.M., et al., *Polymers in focus: fluorescence correlation spectroscopy*. Colloid and Polymer Science, 2014. **292**(10): p. 2399-2411.
46. Woll, D., *Fluorescence correlation spectroscopy in polymer science*. Rsc Advances, 2014. **4**(5): p. 2447-2465.
47. Koynov, K. and H.J. Butt, *Fluorescence correlation spectroscopy in colloid and interface science*. Current Opinion in Colloid & Interface Science, 2012. **17**(6): p. 377-387.
48. Pristinski, D., V. Kozlovskaya, and S.A. Sukhishvili, *Fluorescence correlation spectroscopy studies of diffusion of a weak polyelectrolyte in aqueous solutions*. Journal of Chemical Physics, 2005. **122**(1): p. 9.
49. Jia, P.X. and J. Zhao, *Single chain contraction and re-expansion of polystyrene sulfonate: A study on its re-entrant condensation at single molecular level*. Journal of Chemical Physics, 2009. **131**(23): p. 4.
50. Daniels, C.R., et al., *On the pH-Responsive, Charge-Selective, Polymer-Brush-Mediated Transport Probed by Traditional and Scanning Fluorescence*

- Correlation Spectroscopy*. Journal of Physical Chemistry B, 2013. **117**(16): p. 4284-4290.
51. Zhang, C.F., et al., *Diffusion of Ionic Fluorescent Probes atop Polyelectrolyte Brushes*. Journal of Physical Chemistry B, 2011. **115**(51): p. 15167-15173.
 52. Lehmann, S., S. Seiffert, and W. Richtering, *Spatially Resolved Tracer Diffusion in Complex Responsive Hydrogels*. Journal of the American Chemical Society, 2012. **134**(38): p. 15963-15969.
 53. Raccis, R., et al., *Probing mobility and structural inhomogeneities in grafted hydrogel films by fluorescence correlation spectroscopy*. Soft Matter, 2011. **7**(15): p. 7042-7053.
 54. Vagias, A., et al., *Dynamics in Stimuli-Responsive Poly(N-isopropylacrylamide) Hydrogel Layers As Revealed by Fluorescence Correlation Spectroscopy*. Macromolecules, 2014. **47**(15): p. 5303-5312.
 55. Krichevsky, O. and G. Bonnet, *Fluorescence correlation spectroscopy: the technique and its applications*. Reports on Progress in Physics, 2002. **65**(2): p. 251-297.
 56. Magde, D., W.W. Webb, and E. Elson, *Thermodynamic Fluctuations in a Reacting System—Measurement by Fluorescence Correlation Spectroscopy*. Physical Review Letters, 1972. **29**(11): p. 705-708.
 57. Magde, D., E.L. Elson, and W.W. Webb, *Fluorescence correlation spectroscopy. II. An experimental realization*. Biopolymers, 1974. **13**(1): p. 29-61.
 58. Eigen, M. and R. Rigler, *Sorting single molecules: application to diagnostics and evolutionary biotechnology*. Proceedings of the National Academy of Sciences of the United States of America, 1994. **91**(13): p. 5740-5747.
 59. Yordanov, S., *Total Internal Reflection Fluorescence Cross-Correlation Spectroscopy: theory and application for studying boundary slip phenomenon*, in *Physik, Mathematik und Informatik*. 2011, der Johannes Gutenberg-Universität Mainz. p. 140.
 60. Petrasek, Z. and P. Schwille, *Precise measurement of diffusion coefficients using scanning fluorescence correlation spectroscopy*. Biophysical Journal, 2008. **94**(4): p. 1437-1448.
 61. Jablonski, A., *Efficiency of anti-stokes fluorescence in dyes*. Nature, 1933. **131**: p. 839-840.
 62. AAT_Bioquest. 12/10/2015; Available from: <http://aatbio.com/gen4prst.pl?Cid=1082>.
 63. AAT_Bioquest. Alexa 647. 12/10/2015; Available from: <http://aatbio.com/gen4prst.pl?Cid=1031>.
 64. Loudet, A. and K. Burgess, *BODIPY dyes and their derivatives: Syntheses and spectroscopic properties*. Chemical Reviews, 2007. **107**(11): p. 4891-4932.
 65. Thermofisher. Bodipy. 12/10/2015; Available from: <http://www.thermofisher.com/order/catalog/product/D2184>.
 66. Zrazhevskiy, P., M. Sena, and X.H. Gao, *Designing multifunctional quantum dots for bioimaging, detection, and drug delivery*. Chemical Society Reviews, 2010. **39**(11): p. 4326-4354.

67. Alivisatos, A.P., *Semiconductor clusters, nanocrystals, and quantum dots*. Science, 1996. **271**(5251): p. 933-937.
68. Semrock. *Quantum dots*. 12/10/2015; Available from: <http://www.semrock.com/fluorescence-imaging-with-quantum-dot-nanocrystals.aspx>.
69. Thermofisher. *Quantum Dots*. 12/10/2015; Available from: <https://www.thermofisher.com/de/de/home/references/molecular-probes-the-handbook/ultrasensitive-detection-technology/qdot-nanocrystal-technology.html>.
70. D'Acunzi, M., et al., *Superhydrophobic surfaces by hybrid raspberry-like particles*. Faraday Discussions, 2010. **146**: p. 35-48.
71. Gu, Z.Z., et al., *Infiltration of colloidal crystal with nanoparticles using capillary forces: a simple technique for the fabrication of films with an ordered porous structure*. Applied Physics a-Materials Science & Processing, 2002. **74**(1): p. 127-129.
72. Li, Q., et al., *Porous Networks Through Colloidal Templates*, in *Templates in Chemistry Iii*, P. Broekmann, K.H. Dotz, and C.A. Schalley, Editors. 2009, Springer-Verlag Berlin: Berlin. p. 135-180.
73. Wang, J.J., et al., *Preparation of multilayered trimodal colloid crystals and binary inverse opals*. Journal of the American Chemical Society, 2006. **128**(49): p. 15606-15607.
74. Wang, J., et al., *Structural and optical characterization of 3D binary colloidal crystal and inverse opal films prepared by direct co-deposition*. Journal of Materials Chemistry, 2008. **18**(9): p. 981-988.
75. Jing Xie, K.N., Sayaka Ohno, Hans-Juergen Butt, Kaloian Koynov, Shin-ichi Yusa, *Fluorescence Correlation Spectroscopy Monitors the Hydrophobic Collapse of pH-Responsive Hairy Nanoparticles at the Individual Particle Level*. Macromolecules, 2015. **48**: p. 7237-7244.
76. Biophysics. *8-well chamber*. 12/10/2015; Available from: <http://www.biophysics.com/uSLIDE8well.php>.
77. Thermofisher. *Attofluor Cell Chamber*. 12/10/2015; Available from: <https://www.thermofisher.com/order/catalog/product/A7816>.
78. Edmondson, S., V.L. Osborne, and W.T.S. Huck, *Polymer brushes via surface-initiated polymerizations*. Chemical Society Reviews, 2004. **33**(1): p. 14-22.
79. Barbey, R., et al., *Polymer Brushes via Surface-Initiated Controlled Radical Polymerization: Synthesis, Characterization, Properties, and Applications*. Chemical Reviews, 2009. **109**(11): p. 5437-5527.
80. Kato, M., et al., *Polymerization of Methyl Methacrylate with the Carbon Tetrachloride/Dichlorotris-(triphenylphosphine)ruthenium(II)/Methylaluminum Bis(2,6-di-tert-butylphenoxide) Initiating System: Possibility of Living Radical Polymerization*. Macromolecules, 1995. **28**(5): p. 1721-1723.
81. Wang, J.S. and K. Matyjaszewski, *Controlled/" living" radical polymerization. Atom transfer radical polymerization in the presence of transition-metal complexes*. Journal of the American Chemical Society, 1995. **117**(20): p. 5614-5615.

82. Wang, J.S. and K. Matyjaszewski, *Controlled/"Living" Radical Polymerization. Halogen Atom Transfer Radical Polymerization Promoted by a Cu(I)/Cu(II) Redox Process*. *Macromolecules*, 1995. **28**(23): p. 7901-7910.
83. Matyjaszewski, K., *Atom Transfer Radical Polymerization (ATRP): Current Status and Future Perspectives*. *Macromolecules*, 2012. **45**(10): p. 4015-4039.
84. Matyjaszewski, K. and J.H. Xia, *Atom transfer radical polymerization*. *Chemical Reviews*, 2001. **101**(9): p. 2921-2990.
85. Pyun, J., T. Kowalewski, and K. Matyjaszewski, *Synthesis of polymer brushes using atom transfer radical polymerization*. *Macromolecular Rapid Communications*, 2003. **24**(18): p. 1043-1059.
86. Cherdhirankorn, T., et al., *Tracer Diffusion in Silica Inverse Opals*. *Langmuir*, 2010. **26**(12): p. 10141-10146.
87. Raccis, R., et al., *Confined Diffusion in Periodic Porous Nanostructures*. *ACS Nano*, 2011. **5**(6): p. 4607-4616.
88. Nykypanchuk, D., H.H. Strey, and D.A. Hoagland, *Brownian motion of DNA confined within a two-dimensional array*. *Science*, 2002. **297**(5583): p. 987-990.
89. You, Y.Z., et al., *Temperature-controlled uptake and release in PNIPAM-modified porous silica nanoparticles*. *Chem. Mater.*, 2008. **20**(10): p. 3354-3359.
90. Vasani, R.B., et al., *Stimulus-Responsiveness and Drug Release from Porous Silicon Films ATRP-Grafted with Poly(N-isopropylacrylamide)*. *Langmuir*, 2011. **27**(12): p. 7843-7853.
91. Elson, E., R. Rigler, and E.S. Elson, *Fluorescence correlation spectroscopy - Theory and applications - Introduction*, in *Fluorescence Correlation Spectroscopy: Theory and Applications*. 2001, Springer-Verlag Berlin: Berlin. p. 1-6.
92. Kim, S.A., K.G. Heinze, and P. Schwille, *Fluorescence correlation spectroscopy in living cells*. *Nature Methods*, 2007. **4**(11): p. 963-973.
93. Zettl, H., et al., *Fluorescence correlation spectroscopy of single dye-labeled polymers in organic solvents*. *Macromolecules*, 2004. **37**(5): p. 1917-1920.
94. Bonne, T.B., et al., *Aggregation behavior of amphiphilic poly(2-alkyl-2-oxazoline) diblock copolymers in aqueous solution studied by fluorescence correlation spectroscopy*. *Colloid. Polym. Sci.*, 2004. **282**(8): p. 833-843.
95. Michelman-Ribeiro, A., et al., *Probe diffusion in aqueous poly(vinyl alcohol) solutions studied by fluorescence correlation spectroscopy*. *Biomacromolecules*, 2007. **8**(5): p. 1595-1600.
96. Zettl, H., et al., *Direct observation of single molecule mobility in semidilute polymer solutions*. *Physical Review E*, 2007. **75**(6): p. 6.
97. Gianneli, M., et al., *Local and global dynamics of transient polymer networks and swollen gels anchored on solid surfaces*. *Journal of Physical Chemistry C*, 2007. **111**(35): p. 13205-13211.
98. Woell, D., et al., *Radical polymerization tracked by single molecule spectroscopy*. *Angewandte Chemie-International Edition*, 2008. **47**(4): p. 783-787.

99. Grabowski, C.A. and A. Mukhopadhyay, *Diffusion of polystyrene chains and fluorescent dye molecules in semidilute and concentrated polymer solutions*. *Macromolecules*, 2008. **41**(16): p. 6191-6194.
100. Cherdhirankorn, T., et al., *Fluorescence Correlation Spectroscopy Study of Molecular Probe Diffusion in Polymer Melts*. *Macromolecules*, 2009. **42**(13): p. 4858-4866.
101. Modesti, G., et al., *Diffusion in Model Networks as Studied by NMR and Fluorescence Correlation Spectroscopy*. *Macromolecules*, 2009. **42**(13): p. 4681-4689.
102. Dorfschmid, M., et al., *Translational and Rotational Diffusion during Radical Bulk Polymerization: A Comparative Investigation by Full Correlation Fluorescence Correlation Spectroscopy (fcFCS)*. *Macromolecules*, 2010. **43**(14): p. 6174-6179.
103. Wang, F., et al., *Conformational Transition of Poly(N-isopropylacrylamide) Single Chains in Its Cononsolvency Process: A Study by Fluorescence Correlation Spectroscopy and Scaling Analysis*. *Macromolecules*, 2012. **45**(22): p. 9196-9204.
104. Doroshenko, M., et al., *Monitoring the Dynamics of Phase Separation in a Polymer Blend by Confocal Imaging and Fluorescence Correlation Spectroscopy*. *Macromolecular Rapid Communications*, 2012. **33**(18): p. 1568-1573.
105. Wang, D.P., et al., *Probing Diffusion of Single Nanoparticles at Water-Oil Interfaces*. *Small*, 2011. **7**(24): p. 3502-3507.
106. Mahurin, S.M., S. Dai, and M.D. Barnes, *Probing the diffusion of a dilute dye solution in mesoporous glass with fluorescence correlation spectroscopy*. *J. Phys. Chem. B*, 2003. **107**(48): p. 13336-13340.
107. McCain, K.S., P. Schluesche, and J.M. Harris, *Poly(amidoamine) dendrimers as nanoscale diffusion probes in sol-gel films investigated by total internal reflection fluorescence spectroscopy*. *Anal. Chem.*, 2004. **76**(4): p. 939-946.
108. Lytle, J.C. and A. Stein, *Recent progress in syntheses and applications of inverse opals and related macroporous materials prepared by colloidal crystal templating*. *ChemInform*, 2010. **41**(28).
109. Velev, O.D. and A.M. Lenhoff, *Colloidal crystals as templates for porous materials*. *Current opinion in colloid & interface science*, 2000. **5**(1): p. 56-63.
110. Ramakrishnan, A., R. Dhamodharan, and J. Ruhe, *Controlled growth of PMMA brushes on silicon surfaces at room temperature*. *Macromol. Rapid Commun.*, 2002. **23**(10-11): p. 612-616.
111. Brunger, A.T., *Free R value: a novel statistical quantity for assessing the accuracy of crystal structures*. *Nature*, 1992. **355**(6359): p. 472-475.
112. Enderlein, J., et al., *Art and artefacts of fluorescence correlation spectroscopy*. *Current Pharmaceutical Biotechnology*, 2004. **5**(2): p. 155-161.
113. Mills, R., *Self-Diffusion in Normal and Heavy Water in the Range 1–45 Degrees*. *Journal of Physical Chemistry*, 1973. **77**(5): p. 685-688.
114. Holz, M., S.R. Heil, and A. Sacco, *Temperature-dependent self-diffusion coefficients of water and six selected molecular liquids for calibration in*

- accurate H-1 NMR PFG measurements*. Physical Chemistry Chemical Physics, 2000. **2**(20): p. 4740-4742.
115. Vagias, A., et al., *Complex Tracer Diffusion Dynamics in Polymer Solutions*. Phys. Rev. Lett., 2013. **111**(8): p. 5.
 116. Jochum, F.D., et al., *Thermo- and Light-Responsive Polymers Containing Photoswitchable Azobenzene End Groups*. Macromolecules, 2009. **42**(20): p. 7854-7862.
 117. Zhou, F., et al., *Polyelectrolyte brush amplified electroactuation of microcantilevers*. Nano Letters, 2008. **8**(2): p. 725-730.
 118. Magnusson, J.P., et al., *Ion-sensitive "isothermal" responsive polymers prepared in water*. Journal of the American Chemical Society, 2008. **130**(33): p. 10852-10853.
 119. Andreeva, D.V., et al., *Self-healing anticorrosion coatings based on pH-sensitive polyelectrolyte/inhibitor sandwichlike nanostructures*. Advanced Materials, 2008. **20**(14): p. 2789-2794.
 120. Cavallaro, A., S. Taheri, and K. Vasilev, *Responsive and "smart" antibacterial surfaces: Common approaches and new developments (Review)*. Biointerphases, 2014. **9**(2): p. 10.
 121. Shen, Z., et al., *Thermosensitive polymer-conjugated albumin nanospheres as thermal targeting anti-cancer drug carrier*. European Journal of Pharmaceutical Sciences, 2008. **35**(4): p. 271-282.
 122. Mei, Y., et al., *Catalytic activity of palladium nanoparticles encapsulated in spherical polyelectrolyte brushes and core-shell microgels*. Chemistry of Materials, 2007. **19**(5): p. 1062-1069.
 123. Amalvy, J.I., et al., *Use of sterically-stabilised polystyrene latex particles as a pH-responsive particulate emulsifier to prepare surfactant-free oil-in-water emulsions*. Chemical Communications, 2003(15): p. 1826-1827.
 124. Dupin, D., S.P. Armes, and S. Fujii, *Stimulus-Responsive Liquid Marbles*. Journal of the American Chemical Society, 2009. **131**(15): p. 5386-5387.
 125. Kotsuchibashi, Y., et al., *Construction of 'smart' surfaces with polymer functionalized silica nanoparticles*. Polymer Chemistry, 2013. **4**(4): p. 1038-1047.
 126. Fujii, S., et al., *Surface characterization of nanoparticles carrying pH-responsive polymer hair*. Polymer, 2010. **51**(26): p. 6240-6247.
 127. Li, D.J., et al., *Thermosensitive hairy hybrid nanoparticles synthesized by surface-initiated atom transfer radical polymerization*. Langmuir, 2006. **22**(7): p. 3344-3351.
 128. Yu, F.Q., X.D. Tang, and M.S. Pei, *Facile synthesis of PDMAEMA-coated hollow mesoporous silica nanoparticles and their pH-responsive controlled release*. Microporous and Mesoporous Materials, 2013. **173**: p. 64-69.
 129. Chen, M.Q., et al., *Thermosensitive behavior of poly(N-isopropylacrylamide) grafted polystyrene nanoparticles*. Polymer Journal, 2003. **35**(12): p. 901-910.
 130. Adelsberger, J., et al., *The collapse transition and the segmental dynamics in concentrated micellar solutions of P(S-b-NIPAM) diblock copolymers*. Colloid and Polymer Science, 2011. **289**(5-6): p. 711-720.

131. Kayitmazer, A.B., et al., *Protein-polyelectrolyte interactions*. *Soft Matter*, 2013. **9**(9): p. 2553-2583.
132. Koynov, K. and H.J. Butt, *Particle and Tracer Diffusion in Complex Liquids*. 4th International Symposium on Slow Dynamics in Complex Systems: Keep Going Tohoku, 2013. **1518**: p. 357-364.

Curriculum Vitae

Jing Xie

Master of Science

29. April 1988 in China

Richard Schirrmann Str 14

55122 Mainz

+49 176/82913698

xiechemistry@gmail.com

EDUCATION

10/2012- present **Max Planck Institute for polymer research** Mainz, Germany

Degree to be obtained: Doctor in natural science

09/2009-07/2012 **Jilin University** Changchun, China

Master's degree in polymer chemistry and physics

09/2005-07/2009 **Jilin University** Changchun, China

Bachelor's degree in polymer materials and engineering

CONFERENCE

2th Fluorescence Correlation Spectroscopy in Polymer Science (FCS Workshop),

24th-25th, September, 2015. Aachen, Germany

10th Zsigmondy Colloquium, 07th – 08th, April, 2014. Konstanz, Germany.

15th Conference of the International Association of Colloid and Interface Scientists (IACIS), 24th-29th, May, 2014. Mainz, Germany

PUBLISHED PAPERS

- **Jing Xie**, Mikheil Doroshenko, Ulrich Jonas, Hans-Jürgen Butt, Kaloian Koynov; Temperature-Controlled Diffusion in PNIPAM-Modified Silica Inverse Opals. *ACS Macro Lett.* **2016**, *5*, 190–194.
- **Jing Xie**, Keita Nakai, Sayaka Ohno, Hans-Juergen Butt, Kaloian Koynov, Shin-ichi Yusa; Fluorescence Correlation Spectroscopy Monitors the Hydrophobic Collapse of pH-Responsive Hairy Nanoparticles at the Individual Particle Level. *Macromolecules*, **2015**, *48*, 7237–7244.
- Frank Schellenberger, **Jing Xie**, Noemí Encinas, Alexandre Hardy, Markus Klapper, Periklis Papadopoulos, Hans-Juergen Butt, Doris Vollmer; Direct observation of drops on slippery lubricant-infused surfaces. *Soft Matter*, **2015**, *11*, 7617-7626.
- Alexander Birke, David Huesmann, Annette Kelsch, Martin Weilbacher, **Jing Xie**, Matthias Bros, Tobias Bopp, Christian Becker, Katharina Landfester, Matthias Barz; Polypeptoid-block-polypeptide Copolymers: Synthesis, Characterization, and Application of Amphiphilic Block Copolypept(o)ides in Drug Formulations and Miniemulsion Techniques. *Biomacromolecules* **2014**, *15*, 548-557.